UNIVERSITY OF GHANA

COLLEGE OF BASIC AND APPLIED SCIENCES

SCHOOL OF ENGINEERING SCIENCES

THERMAL ENERGY HARVESTING CHARACTERISTICS OF CALCINED ABONKO CLAY MIXED WITH CHAR FOR BUILDING APPLICATIONS

BY

MICHAEL EFFUI SEWORDOR

(10877021)

THIS THESIS/ DISSERTATION IS SUBMITTED TO THE UNIVERSITY OF GHANA, LEGON

IN PARTIAL FULFILLMENT OF THE REQUIREMENT FOR THE AWARD OF A MASTER OF PHILOSOPHY (MPHIL) IN MATERIALS SCIENCE AND ENGINEERING DEGREE

December 2022

DECLARATION

Candidate's Declaration

I hereby declare that this thesis is a presentation of my original research work and that it was prepared in accordance with all the University of Ghana's rules. Wherever the contributions of others are involved there are efforts to state them clearly and give acknowledgements.

NAME: Michael Effui Sewordor

Signature: …… .. Date: …28th January, 2023….

Supervisor's Declaration

In my capacity as the supervisor of the candidate's thesis, I declare that the organization and presentation of this thesis conform to the University of Ghana's academic rules and that the above statements made by the candidate are true to the best of my knowledge.

Name: Prof. Benjamin Agyei-Tuffour

Signature: … Date: …30th January, 2023……

Head of Department's Declaration

I hereby declare that this thesis has been prepared, administered, and accepted in accordance with the University of Ghana's academic rules. Name: **Professor Abu Yaya**

Signature: .. Date: …30th January, 2023

ABSTRACT

Research into building materials with thermal energy harvesting characteristics has been of prime importance in the past decade, since materials used in building influence the temperature of the room, energy consumption, energy efficiency and the cost of construction. The goal of this research is to investigate the thermal energy harvesting characteristics of bricks made from calcined Abonko clay, Portland cement, and char from palm kernel shells, coconut shells, and acacia wood in various ratios, as well as their mechanical and thermal properties. The composite materials were analyzed using X-ray fluorescence (XRF), X-ray diffraction (XRD), Fourier transformed infrared spectroscopy (FTIR), Thermogravimetric analysis (TGA), Differential scanning calorimetry (DSC), Modulus of rupture (MOR), Compressive strength test and optical and electron microscopy. Furthermore, the heat flow and thermal stresses of the composite bricks were determined using COMSOL Multiphysics modeling and simulations. The compressive strengths showed that the palm kernel char composites (5%, 10% and 15%) recorded values of ~4.60 N/mm^2 , ~4.23 N/mm^2 and ~4.14 N/mm^2 respectively, and these values are higher than the minimum required compressive strength for bricks for construction (~3.5 N/mm^2). The simulation results indicate that the char composites exhibited good energy harvesting characteristics than conventional building materials, with the acacia composite been the most effective. However, the palm kernel char composite experienced lower thermal stress distribution. It was also observed that increasing the percentage of the char in the composite resulted in a lower compressive and flexural strength, nevertheless this had positive influence on the energy harvesting characteristics of the composites. Hence building materials produced from calcined Abonko clay-cement-char composite has the characteristics to maintain thermal comfort and increase energy efficiency in buildings.

Acknowledgements

I give thanks to Almighty God for His mercies and grace throughout my MPhil, particular during the pursuit of my project. I would also want to express my appreciation to my family and friends who supported me in diverse ways to make this project successful. I am very grateful to my supervisor Prof. Benjamin Agyei-Tuffour for his guidance, support, and encouragements in making this project a success. This project wouldn't have materialized if not for laboratory assistance from the Council for Scientific and Industrial Research- Institute of Industrial Research (CSIR-IIR) Materials division technicians especially Messer. Ishmael Aggrey and Kobina Arkaefi, Materials Department, Geological Survey Authority,

Materials Science and Engineering, Physics and Chemistry departments of the University of Ghana, I thank all the staff of these institutions.

Dedication

To God and Family

Table of content

Dedication v

LIST OF FIGURES ix

LIST OF TABLES x

CHAPTER 1 1

INTRODUCTION 1

1.1 Background **1**

1.2 Problem Statement **4**

1.3 Objectives **4**

1.4 Significance of the Research **5**

CHAPTER 2 6

LITERATURE REVIEW 6

2.1 Energy harvesting **6**

2.2 Thermal energy storage **7**

2.2.1 Properties of thermal energy storage materials 9

2.3 Thermal energy storage in building **9**

2.4 Clays **11**

2.4.1 Calcined clays 13

2.5 Agro waste **16**

2.5.1 Palm Kernel 17

2.5.2 Coconut Shells 18

2.5.3 Acacia 19

2.6 Biomass char **19**

2.7 Microstructural Properties **20**

2.7.1 2.7.1 X-ray Fluorescence (XRF) 20

2.7.2 X-ray diffraction (XRD) 20

2.7.3 Scanning Electron Microscopy (SEM) 21

2.7.4 2.7.4 Optical Microscope 21

2.7.5 Thermogravimetric Analyzer (TGA) 22

2.7.6 Differential scanning calorimetry (DSC) 22

2.7.7 Fourier transform infrared spectroscopy (FTIR) 23

2.8 Mechanical Properties **24**

2.8.1 Flexural strength 24

2.8.2 Compressive strength 25

2.9 COMSOL Multiphysics simulations **25**
CHAPTER 3 25
Materials and Methods 26
3.1 Materials and Method **26**
3.1.1 Materials 26
3.2 Materials Preparation **26**
3.2.1 Abonko clay 26
3.2.2 Carbonization of Coconut, Acacia, Palm kernel shells 27
3.3 Composite Preparation and Batch Formulation **29**
3.3.1 Briquettes production 30
3.4 Characterization of Samples **31**
3.4.1 X-Ray Fluorescence 31
3.4.2 X-Ray diffraction 32
3.4.3 Fourier transform infrared spectroscopy (FTIR) 32
3.4.4 Thermal Analysis of Samples 33
3.5 Surface morphology and phase segregation of test samples **33**
3.6 Mechanical Testing of samples **34**
3.6.1 Compressive Strength 34
3.6.2 Flexural Strength 34
3.7 Analytical and Finite Element Modelling **36**
CHAPTER 4 37
RESULTS AND DISCUSSION 37
4.1 Chemical and Mineralogical composition of clay **37**
4.1.1 XRF Analysis of clay 37
4.1.2 XRD Analysis of clay 38
4.2 FTIR Analysis **39**
4.2.1 Control samples 39
4.2.2 Palm kernel char-Calcined Clay-Cement Composite 39
4.2.3 Coconut char-Calcined clay-Cement Composite 40
4.2.4 Acacia char-Calined clay-Cement Composite 40
4.3 Mechanical Properties **41**
4.3.1 Compressive strength 41
4.3.1.1 Palm kernel char-Calcined Clay-Cement Composite and Control 41
4.3.1.2 Coconut shell char-Calcined Clay-Cement Composite and Control 43
4.3.1.3 Acacia Char-Calcined Clay-Cement Composite and Control 43

4.3.2 Modulus of Rupture 43
4.3.2.1 Palm kernel shell-Calcined Clay-Cement Composite 43
4.3.2.2 Coconut shells char-Clay-Cement Composite 44
4.3.2.3 Acacia char-Clay-Cement Composite 44
4.3.3 Thermogravemetric Analysis 45
4.3.3.1 Coconut char-Calcined Clay-Cement Composite 45
4.3.3.2 Palm kernel Char-Calcined Clay-Cement Composite 48
4.3.3.3 Acacia Char- Calcined Clay Composite 50
4.3.4 Differential Scanning Calorimetry 52
4.3.4.1 Control sample 52
4.3.4.2 Palm kernel Char-Calcined Clay-Cement Composite 53
4.3.4.3 Coconut Char-Calcined Clay-Cement Composite 54
4.3.4.4 Acacia Char-Calcined Clay-Cement Composite 56
4.3.5 Microscopic Images 58
4.3.5.1 Control samples 58
4.3.5.2 Palm kernel Char-Calcined Clay-Cement Composite 59
4.3.5.3 Coconut Char-Calcined Clay-Cement Composite 60
4.3.5.4 Acacia Char-Calcined Clay-Cement Composite 61
4.4 Finite Element Analysis (FEA) of Agrowaste Char –Calcined Clay Composites . 62
CHAPTER 5 67
CONCLUSIONS AND RECOMMENDATIONS 67
5.1 Conclusions 67
5.2 Recommendations 67
REFERENCES 68

LIST OF FIGURES

FIGURE 3.1: GAS KILN FOR CALCINATION 27
FIGURE 3.2: (A) RAW ABONKO CLAY (B) PULVERIZED ABONKO CLAY (C) CALCINED ABONKO CLAY.....27
FIGURE 3.3: (A) COCONUT SHELLS (B) CARBONIZED COCONUT SHELLS (C) ACACIA WOOD (D) CARBONIZED ACACIA WOOD (E) PALM KERNEL SHELLS (F) CARBONIZED PALM KERNEL SHELLS (G) CARBONIZATION AND ACTIVATION CARBON PLANT (H) MESH.....29
FIGURE 3.4: (A) WOODEN MOULD (B) MOULD WITH CAST PIECE (C) CAST PIECE (D) DRYING MOULD (E) PRISM WOODEN MOULD (F) PRISM CAST PIECE 31
FIGURE 3.5: TGA/DSC SDT Q600 V20 BUILD 20 MACHINE 33
FIGURE 3.6: AMSCOPE MD 130 MICROSCOPE (B) MICROSCOPY SETUP 34
FIGURE 3.7: (A) HYDRAULIC PRESS (B) TESTED CUBES (C) MOR/5-TS MACHINE (D) TESTED MOR BAR (E) DIGITAL CALIPER 36
FIGURE 4.1: XRD RESULTS FOR RAW AND CALCINED ABONKO CLAY 39
FIGURE 4.2: FTIR RESULTS OF (A CONTROL COMPOSITE (B) PALM KERNEL CHAR COMPOSITE (C) COCONUT SHELL CHAR COMPOSITE (D) ACACIA CHAR COMPOSITE ...42
FIGURE 4.3: COMPRESSIVE STRENGTH RESULTS FOR (A) PALM KERNEL CHAR COMPOSITE (B) COCONUT SHELL CHAR COMPOSITE (C) ACACIA CHAR COMPOSITE 43
FIGURE 4.4: FLEXURAL STRENGTH RESULTS FOR (A) PALM KERNEL CHAR COMPOSITE (B) COCONUT SHELL CHAR COMPOSITE (C) ACACIA CHAR COMPOSITE 46
FIGURE 4.5:TGA RESULTS FOR COCONUT CHAR COMPOSITE (A) 5% ADDITION (B) 10% ADDITION (C) 15% ADDITION (D) 20% ADDITION 47
FIGURE 4.6: TGA RESULTS FOR PALM KERNEL CHAR COMPOSITE (A) 5% ADDITION (B) 10% ADDITION (C) 15% ADDITION (D) 20% ADDITION 51
FIGURE 4.7: TGA RESULTS FOR ACACIA CHAR COMPOSITE (A) 5% ADDITION (B) 10% ADDITION (C) 15% ADDITION (D) 20% ADDITION 53
FIGURE 4.8: DSC RESULTS FOR CONTROL SAMPLE 54
FIGURE 4.9: DSC RESULTS FOR THE PALM KERNEL CHAR COMPOSITE (A) 5% ADDITION (B) 10% ADDITION (C) 15% ADDITION (D) 20% ADDITION 55
FIGURE 4.10: DSC RESULTS FOR COCONUT SHELL CHAR COMPOSITE (A) 5% ADDITION (B) 10% ADDITION (C) 15% ADDITION (D) 20% ADDITION 57
FIGURE 4.11: DSC RESULTS FOR ACACIA CHAR COMPOSITE (A) 5% ADDITION (B) 10% ADDITION (C) 15% ADDITION (D) 20% ADDITION 59
FIGURE 4.12: MICROSCOPIC IMAGE OF THE CONTROL SAMPLE (A)CROSS-SECTIONAL AREA (B)SURFACE OF THE COMPOSITE 60
FIGURE 4.13: MICROSCOPIC IMAGE OF PALM KERNEL CHAR COMPOSITES (A) 5%, (B)10%, (C) 15%, (D) 20% 61
FIGURE 4.14: MICROSCOPIC IMAGE OF COCONUT SHELL CHAR COMPOSITES (A) 5%,(B)10%, (C) 15%, (D) 20%.....62
FIGURE 4.15: MICROSCOPIC IMAGE OF ACACIA CHAR COMPOSITES (A) 5%, (B)10%, (C) 15%, (D) 20% 63

LIST OF TABLES

TABLE 2.1:CHEMICAL ANALYSIS OF STANDARD CLAY MINERALS.....12
TABLE 3.1MATERIALS AND THE LOCATION THEY WERE OBTAINED 26
TABLE 3.2: BATCH FORMULATION FOR CUBES 30
TABLE 3.3: BATCH FORMULATION FOR RECTANGULAR BARS 30
TABLE 4.1: XRF ANALYSIS OF RAW AND CALCINED ABONKO CLAY 39

CHAPTER 1

INTRODUCTION

1.1 Background

The noticeable and ongoing rise in energy demand and consumption is a result of the economy's and society's quick development. As a result, there has been lots of interest in the strategies employed to promote energy efficiency and conservation technologies. This has led to increase in the amount of research being done on various materials that have the potential to store and release large amounts of thermal energy (Li, He, Liu, Cao, & Zhu, 2013).

The increase in the population and the rise in time spent in buildings for office duties, hotels, shopping malls, guest houses and many more has raised urgent concerns for the enhancement of building services to improve comfort levels in buildings, especially in temperate regions. Many technologies have been introduced to meet this demand, including the use of air conditioners, porous and fired bricks, phase change materials, and plasterboards (Zhou, Zhao, & Tian, 2012). Relative to traditional buildings, energy efficient buildings offer a more stable indoor climate, with less draught from windows, walls, floors, and ceiling constructions. Because residents of energy efficient buildings must spend relatively less to heat and cool their homes to within the margins of acceptable comfort, energy efficient construction reduces fuel poverty across society . The need for thermal comfort is driving up the energy consumption of heating, ventilation, and air conditioning systems. In this situation, thermal energy storage technologies that have a high potential for saving energy in buildings have drawn increasing attention (Zhou, Zhao, & Tian, 2012). In France, for instance, the last 30 years have seen an increase in the consumption of energy in buildings to ~30%; these buildings contribute approximately 19% of the total CO_2 emissions in the country(Perez-Lombard, Ortiz, & Pout , 2007) (Kuznik, Virgone, & Johannes, 2011).

A UN conference report presented in 2016 states that, energy demand increases annually by 8% in Africa and 56% of total energy generated is consumed by buildings. Another

significant finding from the research was that big cities in Africa consume over 75% of all electricity produced and accounts for ~70% of greenhouse emissions. The main cause of this problem is the inconsideration in adopting building designs and building codes from western countries (UNHabitat, 2016). It is observed that majority of modern buildings are a replica of western buildings (UNHabitat, 2016).

Ghana, just as other African countries also have energy challenges due to various reasons. The 2015 energy commission report states that the energy demand growth in Ghana is twice as fast as economic growth, due to population growth and the government's desire to build more businesses (Commission-Ghana, 2016). Opoku, Edwin and Agyarko (2019) emphasizes the point that 60-80% of energy used in offices and commercial buildings in Accra and Kumasi is for air-conditioning, this explains how thermal comfort in buildings is very crucial in the life urban dwellers in Accra and Kumasi. The UN report shows that very few urban planners take into consideration passive building methods in their new urban plans ((UNHabitat, 2016).

Therefore, the need for economical and efficient thermal storage materials for building construction that will improve thermal comfort, reduce grid energy consumption, and remain environmentally benign cannot be overemphasized.

Thermal energy harvesting is the process of capturing energy from sources such as thermal, vibration, wind and solar for later use (Selvam, 2019; Enescu, 2019). This reduces the over reliance on nonrenewable fuel sources and contribute to a more efficient and environmentally friendly energy use.

Agricultural waste is a major source of environmental concern in Ghana. It is estimated that 0.2-0.8 kg of solid waste is generated daily per person and 13,500 tons of solid garbage are thought to be involved (Miezah, Obiri-Danso, Fei-Baffoe, Kadar, & Mensah, 2015). Out of this amount, 60% is made up of organic waste, which can serve as a reliable agro-waste char

source for thermal energy storage purposes (Miezah, Obiri-Danso, Fei-Baffoe, Kadar, & Mensah, 2015). Coconut shells, palm kernel shells and acacia trees are agricultural waste commonly available in great quantities in Ghana and tropical Africa. When these agricultural wastes are charred, they enrich the carbon content of the biomass as well as create initial porosities in the material (Mahanim, Asma, Rafidah, Puad, & Shaharuddin, 2011), thereby enhancing the thermal energy harvesting properties.

The availability of clay makes it easy to produce a composite of clay and char to form bricks that will find enormous application in the construction industry in Ghana. There are abundant clay deposits in every district in Ghana, and therefore ensures the availability of raw materials (Yaya, et al., 2018). One of such districts is Abonko in the Mfantsiman municipality in the Central Region of Ghana and has large clay deposit which is one of the industrially explored clays in the country. The deposit is high in plasticity and alumina. The Abonko clay has been utilize extensively in the pottery and ceramics industries to produce earthenware, stoneware, tableware, roof tiles, etc. One of the latest developments in contemporary material science is the advancement of innovative materials and approaches for efficient energy use and the use of sustainable energy sources.

This study investigates the potential of producing composite bricks from calcined Abonko clay mixed with char made from palm kernel shells, coconut shells and acacia wood for effective thermal energy harvesting in Ghana. The study analyzes the composite bricks' thermal heat flow and mechanical properties. Finite Element Analyses (FEA) will be employed to investigate the thermal heat flow and thermal stress distributions using COMSOL Multiphysics Software which will be compared with experimental work to determine the composite bricks' thermal behaviour and strength properties.

1.2 Problem Statement

In recent years, the high-rate energy consumption, and emissions from buildings in both warm and humid regions worldwide have raised eyebrows on materials used in constructing buildings. The high energy consumption can be attributed to energy loss in buildings due to weakened structural components, including windows, doors, walls, floors, and insulation. For instance, 35% of energy is lost through the walls of buildings through conduction, convection, and radiation (Wargorcki, et al., 2006). Moreover, this will inevitably occur since most of building materials used in construction lack thermal energy harvesting characteristics. The rapid population growth, increased demand for building services, time spent in building and the desire to have optimum comfort in buildings is making the end user request more. Due to the lack of comfort and fluctuating room temperatures in buildings, most people have sorted out the use of air conditioners to resolve this problem, hence the increase in the cost of building and energy consumption.

In many developing countries, where agriculture is a key proponent in the daily life of the people it is important to have measure that will curtail the pollution of the environment from waste generated from agriculture. When these wastes from agriculture are not well managed, greenhouse gas are emitted into the environment from burning these waste, unpleasant odors are created and toxic liquids can be infiltrated into water sources. Therefore, the current study seeks to develop not only an inexpensive building material but one with sufficient thermal energy storage characteristics, enhanced mechanical strength to reduce the high energy consumption associated with the use of air conditioners as the prime option to attaining thermal comfort in buildings.

1.3 Objectives

The objectives of this study were:

The main objective of this research is to produce bricks from calcined Abonko clay mixed with carbonized materials made from agro waste to enhance thermal energy harvesting and investigate their potential in energy harvesting in buildings.

The specific objectives of this project are to:

- To formulate composite bricks with calcined Abonko clay mixed with carbonized materials (palm kernel, coconut shells and acacia) with good energy harvesting characteristics for building applications.
- To determine the microstructural, mechanical, and thermal energy harvesting characteristics of the composite bricks
- To model the mechanical and thermal stress distributions in the calcined Abonko clay composites using finite element methods.

1.4 Significance of the study

The prime aim of this work is to produce alternative composite building materials from calcined clay mixed with char. The findings from this research work would be used as an ecofriendly building material with good thermal energy harvesting characteristics. These thermal energy storage materials will also help to reduce CO_2 emissions from buildings because there will be a reduction in the use of ordinary Portland cement in the brick formation. Due to the good thermal conductivity of the storage materials, energy efficiency will increase, and the temperature of rooms will be constant to meet thermal comfort criteria. Additionally, environmental pollution from agro-waste which is a major menace in the country would be solved since these agro-wastes would be used as raw materials to produce the composite. Utilizing these wastes would benefit the country economically and aid in environmental pollution control (Aigbodion, et al., 2008).

CHAPTER 2

LITERATURE REVIEW

2.1 Energy harvesting

As non-renewable fuel source resources become less accessible and high-priced, many energy preservation actions have become increasingly practicable (Dilip & Marika, 2009). Even though energy conservation is very publicized and studied, peak load strength management was not properly focused on until recently, (Reindel, 1996; Riyadh, 1997). Peak demand is critical because utility providers must either invest in new generation capacity or purchase electricity from neighboring countries to prepare for the expected increase in peak demand. Peak load energy is more expensive to produce because it is generated by older, less efficient generators that use more and more expensive fuels like oil or gas (Hasnain, 1998).

In the last ten years, the energy harvesting field has been progressively enhanced; the rising number of articles and journals are evidence. Several wonderful review items have been written on this issue, covering various techniques and methods (Liu, Junwen, Chengokuo, Seung-Wuk, & Liwei, 2018). Energy harvesting is the direct conversion of environmental energy such as wind, solar and thermal into electrical energy by the aid of certain materials, devices, and transformation mechanism (Bowen, Tropolov, & Kim, 2016). Energy harvesting is defined as the collection of energy from the environment for local use (Kiziroglou et al., 2012). The concept of multi-modal energy harvesting has been pursued to efficiently harvest energy from unlimited environmental resources. This concept enhances existing systems by incorporating the following principles: (i) two or more energy harvesting sources, such as solar, wind, and vibration, may be available for harvesting energy, and (ii) two different energy harvesting schemes can be combined in one system so that one aids the other (Kiziroglou & Yeatman, 2012).

2.2 Thermal energy storage

Thermal energy storage electronics can play an important part in changing power use patterns for warming. Warm energy storage is critical in many engineering applications. Among the practical issues involved in solar energy systems is the need for an effective means of storing, preserving, and later releasing excess heat collected during bright sunlight for use during the night or other periods. The availability and utilization of waste heat might cause similar issues with waste heat recovery systems. Heat storage can once again be used in most constructions where heating needs are critical, and electricity rates allow heat storage to be competitive with other forms of warming (Sheng, et al., 2022).

The two basic types of thermal energy storage techniques are sensible and latent heat storage. A sensible heat storage system achieves storage by increasing the temperature of the medium, usually a solid or liquid, so that sensible storage materials do not change in phase over the temperature range of the storage process. Sensible heat storage in a material is significantly influenced by its heat capacity, rcp, which influences energy density, and thermal diffusivity, k/rcp, which determines the rate at which heat can be released and recovered. The amount of energy stored is given by the following equation: $Q = mC_p\Delta T$ where, Q is the energy stored, m is the mass of the storage medium, cp is the specific heat of the material and ΔT is the temperature change during the process (Kuravi, Trahan, Goswami, Muhammad, & Stefanakos, 2013). While latent heat storage primarily depends on heat absorption or release when a storage material transitions from solid to liquid, liquid to gas, or vice versa (Pasupathy, Velraji, & Seeniraj, 2008). The storage capacity of a latent heat system is determined not solely by the specific heat of the material, but also by the enthalpy of phase transition, which may allow for a smaller, more efficient, and lower-cost alternative to sensible heat thermal storage systems (Kuravi, Trahan, Goswami, Muhammad, & Stefanakos, 2013). The storage medium's temperature is raised to achieve sensible heat storage. Thus, a

storage medium with a high specific heat capacity, general balance under thermal control, and most importantly, high efficiency is advantageous. Sensible heat storage may be classified based on the heat storage media as liquid media storage like water, oil-based, liquids, molten salts and solid media storage (like rocks, metals, and others). Latent heat storage is a specifically attractive method because it supports an extreme energy storage density and can store heat as latent heat of fusion at continual hotness, matching the phase change temperature of the phase change materials.

When undergoing a phase transition process (e.g., solid-liquid),phase change materials absorb and release heat at a constant temperature and have a high heat of fusion and high thermal energy storage densities compared to other sensible heat storage materials. Organic and inorganic phase change materials are the two types of phase change materials. Organic phase changed materials are a very important class of materials because of their unique thermal properties such as congruent melting and narrow melting/freezing temperature range. These properties make them suitable for many applications in solar energy storage, textiles, and cooling of electronic devices. Organic phase change materials are the most suitable materials for cooling/heating of building (R.K, Ganesan, Tyagi, Metselaar, & Sandarian, 2015).

Phase change materials undergo solid/solid, liquid/gas, and solid/liquid phase transformations. Few solid/solid phase change materials that have heats of fusion and transition temperatures suitable for thermal storage applications have been identified. Liquid/gas phase change materials usually have high heat of transformations, and however, due to the large volume change during transformation, they are not usually considered for practical applications. Solid/liquid Phase change materials are useful because they store a relatively large amount of heat over a narrow temperature range without a large volume change. Liquid/gas Phase change materials usually have high heat of transformations, and however, due to the large volume change during transformation, they are not usually considered for practical applications. Solid/liquid Phase change materials are useful because

they store a relatively large amount of heat over a narrow temperature range without a large volume change (Hasnain, 1993). Thermal energy storage can be accomplished through either sensible or latent heat storage. For generations, architects have used sensible heat storage to store and release passive thermal energy. However, unlike latent heat storage, a much larger capacity of the material is required to store the same amount of energy (Hasnain, 1998).

2.2.1 Properties of thermal energy storage materials

The properties of a material define its use and purpose; therefore materials used for energy storage have peculiar characteristics. For instance, suitable phase change temperature, a large melting enthalpy, and a limited volume change of phase change (D'Alessandro, et al., 2018). This material must possess characteristics such as high latent heat storage capacity, good thermal conductivity, low cost, phase separation, resistance to corrosion and super-cooling phenomenon (Shafigh, Asadi, & Mahyuddin, 2018). For thermoelectric materials to be excellent thermal energy storage materials they should have high Seebeck coefficient and electrical conductivity simultaneously, as well as low thermal conductivity (Cai et al. 2013 & Dollfus et at. 2015).

Piezoelectric materials are another area of interest in thermal energy storage due to their ability to convert mechanical energy into electrical. For these materials to be effective and efficient in energy storage, they must have high dielectric constant, low dielectric losses, excellent piezoelectric properties, piezoelectric coefficient, poling condition, and environmental friendliness (Huang et al. 2009 & Liu et al. 2017).

2.3 Thermal energy storage in building

With growing concern on the practices that harm the environment, as well as exorbitant costs of new power plants, new approaches to construction technologies are required to halt this increase in power consumption. The use of building materials such as cement blocks, concrete, bricks, adobe blocks, steel, plaster, and other building materials have not been able

to adequately address the challenge of high energy consumption in buildings. For these reasons alternative materials are being explored.

Phase change materials are one of these new materials been explored, researchers have explored the possibility of infusing phase changed materials into concrete, cement blocks and plaster boards. In 2016, Mahkamov successfully infused phases change materials into gypsum wallboard to increase thermal energy storage capacity in buildings, with a focus on peak load shifting (Mahkamov, 2016). Some composites materials have been fabricated using readily available and low-cost materials such as coarse aggregates, sand, gypsum, cement, vermiculite, and polyester resin. Six potential thermal energy storage applications for phase change materials for energy conservation in buildings have been identified (Zhou et al. 2012). Phase change materials are encapsulated into ceilings, floor, concrete, or gypsum wallboard of buildings for passive heating and cooling (Kenisarin & Mahkamov, 2016). This practice increases the energy storage capacity of the building, improves the inhabitant comfort level by up to 32% and reduces temperature fluctuations (Ramakrishnan, Wang, Sanjayan, & Wilson, 2017).

Wang et al., (2018), outlined electromagnetic, piezoelectric, thermoelectric, solar and pyroelectrics as the five current types of energy harvesting materials (Wang, Jasim, & Chen, 2018). Since many parts of the buildings are in direct contact with the sun, civil engineering now utilizes facades such as smart windows, ceramics, curtains, and fabrics to capture the sun's energy (Luciana Sucupira, 2021).

Thermoelectric materials based on cement have also found use in energy harvesting; these materials convert heat absorbed by the building surfaces into electrical energy which is used later. Thermoelectric materials improve building internal atmosphere, energy consumption with interior thermal comfort (Ghosh, Harish, Rocky, Ohtaki, & Saha, 2019).

Various additives are added to cement to alter its properties to make it valuable in energy harvesting in buildings, while keeping their structural properties and making them

multifunctional (Gibson, 2010). Carbon-based structural composites, structural capacitors, phase changed materials, thermoelectric-based cement composites, graphite and graphene composites, steel fiber composites, CF composites and carbon nanotubes/nanofibers have been explored for energy harvesting in buildings (V.P. Singh, 2021).

2.4 Clays

Clays are categorized according to their mineralogical and physical properties and potential applications. Clays are fine-grained with particle sizes less than 2 µm and differ greatly in their water and impurities in their composition. Clays are plastic when wet, hard when fired and are used widely for decorative and industrial purposes. These applications arise from the fact that they are locally available, easy to acquire, harmless to human health, stable and recyclable (Savic, 2014).

Clays are classified as primary and secondary according to the mode of formation. Primary clays are those formed in situ whereas secondary clays are depositional. Clays are classified as kaolinite, illite, montmorillonite, smectite, talc and vermiculite. However kaolinite, illite and montmorillonite are referred to as standards clay minerals (Mitchell, 2005; Lombardi, 2002). Kaolinites are alumino-silicate minerals formed by stacking layers composed of alternating tetrahedral and octahedral sheets (Rodrigo, Martirena, & Scrivener, 2011). Kaolinite has a chemical formula $Al_2Si_2O_5(OH)_4$; kaolinite clays are made up of two separate sheets with interlayer surfaces that coexist: one with aluminate groups and one with silicate groups. Al-OH and Si-O groups from the aluminol and siloxane molecules form hydrogen bonds that connect the neighbouring layers. These interlocking forces mean kaolin is non-swelling clay (Billhall B.T. & Partyka, 2011). Furthermore, in the plane of atoms shared by both sheets, two-thirds of the atoms are oxygen and one-third is hydroxyls.

The unit layer in illite and montmorillonite clay structures are formed by an octahedral sheet of alumina sandwiched between two sheets of silicon tetrahedron. As a result, the adjacent

interlayer surfaces are similar and only composed of siloxane groups; however, the nature of the interlayer bond differs from that of kaolinite. Because aluminium fills about one-fourth of the silicon positions in illite, the resulting charge deficiency of 1.3 - 1.5 per unit cell is balanced by potassium between the layers, forming a strong bond (Lombardi, 2002).

Montmorillonite has a crystal structure like illite, except that, isomorphous substitution usually occurs in the octahedral sheet where every sixth aluminium is replaced by magnesium. Various cations, such as sodium or calcium, form adsorption complexes with water molecules, resulting in a balance charge between successive layers. These bonds are frail and easily broken by cleavage or adsorption of other polar liquids. As a result, the position and number of hydroxyl groups vary greatly between structures. Table 2.1 is a chemical analysis of standard clay minerals (Lombardi, 2002).

Table 2.1: Chemical Analysis of Standard Clay Minerals

% Weight	SiO_2	Al_2O_3	Fe_2O_3	CaO	MgO	SO_3	K_2O	MnO	Na_2O	LOI	Total	$\%Na_2O$
Kaolinite	48.0	36.4	0.9	0.1	0.1	0.03	0.5	0.01	0.02	13.4	99.5	0.3
Illite	58.7	19.3	5.0	1.3	2.5	0.2	6.1	0.1	0.2	5.7	99.1	4.2
Montmorillonite	63.2	20.1	4.0	1.2	2.3	0.5	0.5	0.0	2.2	5.9	99.9	2.6

As of 1985 the Ghana Geological Survey Authority had undertaken significant research on clay deposits and discovered that clay existed in commercially exploitable quantities in most of the districts in the country (Sarfo-Ansah, 2010). Clay minerals are accumulated across all the regions in many areas of Ghana, and they are mostly from residual origins (Yaya, et al., 2018), some of the major secondary clay deposits are Abonko, Ochiso, Baifi, Essuakyir No.2, Ekon, Fomena, Saltpond and Mankessim in the Central region of Ghana, Oyibi in the Greater Accra region, Tanoso in Ahafo region, Adidome, Kpeve and Kadjebi in the Volta region and Asokwa, Mfensi and Afari in the Ashanti region.

Some well-known primary clay deposits in Ghana are Teleku-Bokazo, Wassa and Aluku in the Western region, Saltpond clay in the Central region, Anfoega in the Volta region and Kibi (Kyebi) in the Eastern region (Yaya, et al., 2018; Hammond, 1997).

Clay minerals in Ghana differ in properties due to the presence of impurities, hence promoting different applications (Appiah, Indome, & Fudzi, 2014). Most Ghanaian clays are coloured and this colourization is largely due to the presence of iron in the framework of the clay and chemical interaction with organic matter in the environment (Al-Juboury, 2009). Major uses of the resource in Ghana are for brick production, tiles, and medicinal purposes (Mohammed, 2010). Clays in Ghana are currently used for several products, including building bricks, insulation bricks, roofing tiles, facing tiles, pavement tiles and assay crucibles (Yaya et al., 2018).

2.4.1 Calcined clays

Clay calcination is the process of heating clay minerals to high temperatures to convert them to reactive metakaolin. This procedure removes water and chemically bonded crystalline structures from the clay at temperatures ranging from 500°C to 800°C. During heating, three processes occur: dehydroxylization, calcination, and crystallization (Mendelovici, 1997). Wolters et al. (2007) affirms Mendelovici discovery that when raw clays are heated, three major phenomena related to the aluminosilicate material can be differentiated: dehydration, dihydroxylation and recrystallisation (Wolters & Emmerich, 2007).

Dehydration is the release of molecular water that is either adsorbed inside the pore structure or related with the interlayer cations seen in most 2:1 clay minerals (Wolters & Emmerich, 2007). Dehydroxylization is the process of breaking down crystal structure and this can render the clay partially disordered and reactive. During dehydroxylization, octahedral sheets lose water and transform into a meta-stable state (Mendelovici, 1997). Clay minerals with lower crystallinity exhibit dihydroxylation effects at lower temperatures and within a wider

temperature range, compared to similar clay minerals with a higher crystallinity due to wide ranging bond energy distribution for hydroxyl groups (Ptacek, 2013). As shown by Frost et al., that at temperatures above 850°C, recrystallization phenomena takes place, indicating the conversion of structural disordered, potentially reactive phases to more stable, high temperature phases which exhibit no pozzolanic reactivity (Frost & Vassallo, 1996).

Calcination is commonly used to achieve thermal activation; thermal activation of clay minerals causes them to react with Portland cement during hydration. These thermally activated clays become more reactive with cement at appropriate calcination temperatures, improving the strength and durability of concrete. Temperatures ranging from 500°C to 900°C have been found to be optimal for the production of reactive clays (Hellar-kallai, 2006). However, the origin, chemistry, quantity and type of impurities of the clay will determine the precise calcination temperature needed to thermally activate the clay (Guggenheim & Martin, 1995).

Calcination of kaolinite clays into metakaolin makes the clay structure highly disordered, offering good properties as a mineral additive in cement and concrete production (Sigh M. & Grag, 2006). This disorder is due to the re-organization of the Al-O network in the clay (Kakali, Perraki, Tsivilis, & Badogiannis, 2001). The calcination temperature also influences the environment of the layered silicate, which is also an indicative of the reactivity of calcined clays (Fernadez et al., 2011). At high temperature, the clay minerals begin to crystalize, which decreases reactivity. At approximately 600°C, kaolintic clays fully dehydroxylize, while the smectite and the illitic groups dehydroxylize above 600°C, this explains the differences in the calcination temperature (Mendes, Gates, Sanjayan, & Collins, 2011). Calcination helps to optimize the pozzolanic reactivity of metakaolin for potential industrial applications **(**Sigh M. & Grag, 2006; A., Kovler, Grader, & Shter, 2003).

The calcined clay is an important and well-researched material that is used as a supplementary cementitious material (SCM) in concrete production (Bediako, Shrikant, & Kevern, 2017). The potential use of metakaolin (calcined clay) in concrete has been well established; for example, it has been shown that the replacement of cement with 5 wt% – 10 wt% of metakaolin can drastically improve the mechanical properties of concrete, as well as its durability (Billhall & Partyka, 2011). Research in concrete and cement has shown that kaolinite clays are the most reactive type of clay; however, most of these works looked at the influence of calcination parameters such as time and temperature on the properties of the cement. Pozzolanic materials are typically fine aluminosilicates that chemically react with calcium hydroxide to form additional calcium silicate hydrate and other cementitious compounds.

Research on how different clays' pozzolanic characteristics are affected by the decomposition process; metakaolin has been the subject of numerous studies since it is calcined clay that is well known for being extremely reactive. The mineral makeup and calcination temperature of any clay after it has been calcined determine how reactive it is (Badogiannis E., Kakali, & Tsivilis, 2005). Surana et al. confirm Badogiannis et al. research on the factors that influence the development of pozzolanic properties in fired clays. He further goes on to find out that the fineness of the clay also influences the pozzolanic properties. Research into cements and concretes has looked at the pozzolanic properties of various calcined clay minerals by mixing them with lime or cement, and the various researches concluded that kaolinite is the most reactive type of clay for a complete reaction to take place (He, Osabaeck, & Makovicky, 1995). However, it is worth noting that the clay should be grounded before calcination (Ambroise, Murat, & Pera, 1985).

The calcined clay's greater water need can partly be attributed to its effect on compressive strength. As a result, the water supply for the cement is reduced. Secondly, calcined clay

offers soluble alkali silicon and aluminium ions that increase the pozzolanic reactivity of the clay and result in the formation of new calcium silicate hydrate (CSH) and calcium aluminate hydrate (CAH) phases (Fernandez, Martrena, & Scrivener, 2011). Additionally, because calcined clays release ions at a faster pace than fly ash and other Type II additions do, they begin to work as early as seven days after being installed as a cement replacement (Sybertz, 1993). For kaolinite, dehydroxylation can be finished at 600°C because there are hardly any hydroxyls left in the sample after such thermal treatment. For illite clays, dehydroxylation occurs between 600 and 800°C, whereas for montmorillonite, dehydroxylation happens between 600 and 900°C, indicating that the structure is not totally dissolved.

All peaks belonging to kaolinite would have vanished from typical kaolinite clay calcined at 600°C, according to XRD patterns, showing a very severe loss of crystallinity. Due to its higher hydroxyl group content and where they are located in the clay's crystal structure, which favours more disorder and exposes Al (5) groups at the material's surface during the dehydroxylation process, kaolinite was shown to have the highest potential for activation. (Fernandez, Martrena, & Scrivener, 2011).

2.5 Agro waste

The administration of municipal solid waste is a major challenge in many parts of the developing world. There are significant worries about achieving the Sustainable Development Goals due to rising population and urbanization, as well as the extremely high rate of waste generation. The World Bank estimates that there were approximately 3 billion urban dwellers globally in 2012, producing 1.3 billion tons of solid trash annually. Waste generation in subSaharan Africa was estimated to be 62 million tons per year, or 0.65 kilograms per person per day. (Hoornweg & Bhada-Tata, 2012).

The ineffective management of municipal solid garbage is an unresolved problem for Ghanaian municipal officials. Large cities produce 2000 tons of mixed municipal garbage every day, of which 80% is collected and dumped at open landfills or the few available

landfills. Of this waste, 60% is organic (Cofie O., Rao, Fernando, & Pau, 2009). In Ghana, there are currently between 0.2 and 0.8 kilograms of solid trash produced per person every day, totaling around

13,500 tons produced nationwide (Miezah, Obiri-Danso, Kadar, Fei-Baffoe, & Mensah, 2015). The influence of waste landfill emissions on global warming, the burden of gastrointestinal disorders, indiscriminate garbage dumping, especially in developing countries, and the high expense of waste treatment have all been overwhelming (Starovoytova, 2018), as a result, socially and environmentally acceptable waste management approaches are being used to improve public health and resource efficiency (Vergara & Tchobanoglous, 2012).

Among the agricultural wastes produced in Ghana each year are coconut and palm kernel shells, which are byproducts of the oil palm and coconut, respectively (Tsai, Lee, & Chang, 2006). Electricity can be produced from agricultural waste, and these agricultural wastes can also be used for thermal energy, cement replacement in concrete, energy-efficient construction materials, soil stabilization, and in cement production, green building materials. Using these waste materials can reduce the environmental impact of waste disposal and create more value from solid waste materials (V., Ralegaonkar, & Mandavgane, 2013) (Prusty J. K., Patro, & Basarka, 2016).

Kazmi et al. (2016) examined the replacement of rice husk and sugar cane bagasse ashes (agro waste) in clay brick production at replacement rates of 5, 10, and 15%. Although the bricks had substandard mechanical qualities, adding 5% sugar cane bagasse or rice husk ash allowed them to still meet the standards (Kazmi, Abbas, Saleem, Manir, & Khitab, 2016).

2.5.1 Palm Kernel

In Ghana, it is projected that 2,469,763 tonnes of palm oil are produced annually; during peak seasons, up to 30 tons of palm fruits can be produced per hectare per month; and during lean

seasons, approximately 2.2–3.3 tons can be produced (Ofosu-Badu & Sarpong, 2013). Although palm kernel waste has recently been shown to be a viable source of energy, industries consume significantly more waste (palm kernel husk) than is produced by oil producers (Bediako, Gawu, Adjaottor, Ankrah, & Atiemo, 2016). There are huge amounts of this palm kernel husk waste dumped in the sites and around many palm oil production areas in the country. Palm kernel is used as a raw material to produce activated carbon, aggregate of concrete, and used in the preparation of pozzolana.

2.5.2 Coconut Shells

Coconut shells and palm kernel shells are rich in organic constituents (cellulose, hemicellulose, and lignin) and have high energy content. Coconut shells have little or no economic value, and disposing of them is not only expensive but may also cause environmental issues. Due to its excellent natural structure and low ash content, coconut shell is ideal for preparing microporous-activated carbon (Daud, Ali, & Sulaiman, 2000). Carbonization is used to enrich carbon in a material and create initial porosity. High carbonization temperatures have been found to cause many volatiles to be released from the raw material, which can eventually affect product yield and porosity. Cellulose decomposes at temperatures ranging from 200 to 400°C, whereas lignin decomposes at temperatures ranging from 150 to 750°C. Researchers have already established that lignin begins to decompose at low temperatures (160-170°C) and continues to decompose at a slow rate until around 900°C. In a narrow temperature range of 200 to 400°C, hemicellulose is the second component to begin decomposing, followed by cellulose. This is the interval during which the majority of the decomposition occurs in the biomass pyrolysis process, which consists of degradation reactions. Beyond 400°C, the aromatization process is the most important reaction, with a low mass loss rate (Mackay & Roberts, 1982)

2.5.3 Acacia

Acacias are native to tropical and subtropical regions of the world, most notably Australia (where they are known as wattles) and Africa, where they are well-known veld and savanna landmarks.

Acacia leaves are distinguished by small finely divided leaflets that give the leafstalk a feathery or fernlike appearance. Several acacia species are economically significant. Gum acacia (Acacia Senegal), which is native to Africa's Sudan region, produces true gum arabic, which is used in adhesives, pharmaceuticals, inks, confections, and other products. The bark of most acacias contains a high concentration of tannin, which is used in tanning as well as dyes, inks, pharmaceuticals, and other products. Several species, including the Australian Blackwood and the Australian yarran produce valuable timber.

2.6 Biomass char

Biochar's are stable solid materials with a high carbon content, low density, and high porosity. High carbon content, specific surface area, high energy density, developed porous structure, hydrophobic, brittle, and less agglomerate are some of the properties of biomass char that have led to its widespread use in a variety of applications. (Khiari, Jeguirim, Limousy, & Beennici, 2019). For example, biomass chars are used in reducing contaminants in soil (Uchimiya M, et al., 2010), reduction of nutrient loss (Yao, et al., 2011), improvement of soil properties (Carrier M, Hardie , Uras, Görgens , & Knoetze , 2012), waste water treatment (Zhang C, et al., 2013) , gas separation and energy storage (González AS, Plaza ,, Rubiera , & Pevida , 2013). Although traditionally biomass char has been used for soil amendments in agriculture, currently, they have found great use in energy storage due to their physical, chemical, texture, morphology properties (Khiari, Jeguirim, Limousy, & Beennici, 2019) and high performance in energy storage than conventional systems (Xiu S, Shahbazi , & Li , 2017). However, one major disadvantage of biomass chars is their high price and limited supply when compared to fossilbased carbonaceous resources (Norgate TEL, 2009).

These biomass chars are produced by pyrolysis, gasification, hydrothermal carbonization, and torrefaction and the char's characteristics depend on the initial raw material and the production process (Khiari et. al, 2019).

2.7 Microstructural Properties

2.7.1 2.7.1 X-ray Fluorescence (XRF)

X-ray fluorescence (XRF) is a non-destructive analytical technique used to determine the elemental composition of materials. The chemistry of a sample is determined by the XRF analyzer by measuring the fluorescent X-rays produced by the sample after stimulation with the main X-ray source. Each component in a sample emits a unique set of distinguishing fluorescent X-rays, making XRF spectroscopy an excellent technology for qualitative and quantitative material composition analysis. When X-ray radiation interacts with materials, electrons move in and out of them. Their shell levels and XRF peaks in the spectrum, each with a different intensity are emitted. In a graph depicting X-ray intensity peaks as a function of energy peaks, the element can be identified by the peak energy, and the peak height or intensity typically indicates its concentration. XRF is used in the oil and gas, metal fabrication, automotive and aerospace, scrap metal recycling, mining and exploration, construction, and environmental engineering industries to identify and quantify contaminants and detect elements (Fisher, Hajaligol, Waymack, & Kellog, 2002).

2.7.2 X-ray diffraction (XRD)

X-ray diffraction is a non-destructive technique for determining the atomic structure of crystalline objects using elastic scattering. Because of their extremely short wavelength, hard x-rays are required to identify atomic details.

It is a technique that is frequently used in geology, material science and biology for identifying and characterizing unknown crystalline minerals. Diffraction occurs when a periodic array with long-range order scatters light, resulting in constructive interference at

specific angles. When X-rays from atoms scatter, they reveal details about the arrangement of atoms within the crystal. The distance between parallel atom planes determines the position of the diffraction peaks. The diffraction pattern is influenced by a material's distinct crystal structure.

2.7.3 Scanning Electron Microscopy (SEM)

A scanning electron microscope, for example, is used to produce images of a sample by scanning with a focused, high-energy electron that interacts with the atoms in the sample. Backscattered electrons (BSEs) are produced during scanning and travel directly toward the detector; this signal (electrons) is converted into photons by accelerating the electrons and striking them against a disk. The photons then pass through a light guide before entering a photomultiplier tube for signal gain, which is amplified further for display on a display screen. The display image depicts the surface topography, composition, and other properties of the sample. Modern SEM images are digitally recorded; that is, the intensity of signal electrons for each pixel is digitized and saved on a computer as a digital file for each scan. The digital imaging capability enables the generation of an image by averaging multiple scans for the same area. Furthermore, a frame-averaging method can reduce imaging background noise (Naresh Marturi, 2014).

2.7.4 2.7.4 Optical Microscope

Optical microscopes are instruments that enlarge (by the aid of a visible light and a set of lenses) very small samples that the human eye cannot. The eye pieces lens ultimately magnifies the image obtained, before sending it to the retina and to the camera's film plane, the surface of a computer chip with light sensitivity (Kaufmann, 2003). Although various intricate designs strive to improve sample resolution and contrast, optical microscopes are often simple. Normal light-sensitive cameras can use the image from an optical microscope to create a micrograph (Mertz, 2019).

The functions of an optical microscope include image formation, magnification, and resolution.

2.7.5 Thermogravimetric Analyzer (TGA)

Thermogravimetric Analysis **(**TGA) is a material characterization method used in a variety of petrochemical, food, pharmaceutical, and environmental applications. TGA continuously monitors the mass of the substance as the temperature is linearly increased and physical properties such as mass change or enthalpy change. A precision balance supports a sample pan, which is the main component of a TGA; the pan in the furnace is heated or cooled throughout the experiment.

The experiment measures the mass of the sample and manages the sample environment with a purge gas. This gas may be inert or reactive as it passes over the sample and exits through an exhaust. TGA is used to determine the thermal stability of a substance, the decomposition mechanism of inorganic salts, qualitative analysis, evaporation rates of different liquid mixtures, quantitative analysis, moisture and volatiles content of materials, and polymer analysis. TGA can be used to investigate the following processes: evaporation, sublimation, oxidation, decomposition, desorption, and adsorption. Thermal analysis techniques are based on the dynamic relationship between temperature and weight change. TGA can study processes that occur as a result of a mass change; however, it cannot study processes such as melting, transitions from one crystalline form to another, or glass transition temperature (Brown, 2007).

2.7.6 Differential scanning calorimetry (DSC)

Differential scanning calorimetry is the most used thermal analysis method (DSC). When the physical and chemical properties of a sample change as a function of temperature or time, DSC measures the enthalpy changes that occur as a result of those changes. Differential Scanning Calorimetry (DSC) measures the difference in heat flow rate between a sample and

a reference sample. At the same time, they are subjected to a temperature control program (Hohne,

Hemminger, & Flammersheim, 2003)When a sample absorbs or releases heat as a result of thermal effects such as melting, crystallization, chemical reactions, polymorphic transitions, vaporization, and many other processes, differences in heat flow occur. The difference in heat flow can also be used to determine specific heat capacities and changes in heat capacity, for example, during a glass transition. Thermal effects can be quickly identified across a wide temperature range, and the relevant temperature and characteristic caloric values can be calculated using substance quantities in the mg range. DSC measurement values allow for the determination of heat capacity, heat of transition, kinetic data, purity, and glass transition. DSC curves are used to identify substances, create phase diagrams, and calculate crystallinity (Hohne, Hemminger, & Flammersheim, 2003). DSCs enable the measurement of reaction heats and heats of transition, as well as heat flow rates and their changes at specific temperatures, on small sample masses (milligram range; gram range for classic calorimeters), over wide temperature ranges, and with an accuracy that is usually sufficient for the purpose. DSCs are used in the following fields: material characterization, comparison measurements, quality control, substance identification, stability investigations, phase diagram evaluation, purity determinations, kinetic investigations, safety investigations, and heat capacity determination (Hohne, Hemminger, & Flammersheim, 2003). In addition to measuring heat, DSCs are used to measure heat flow rates (power) and characteristic temperatures of a reaction or a transition.

2.7.7 Fourier transform infrared spectroscopy (FTIR)

The Fourier transform infrared spectroscopy (FTIR) employs mathematics to convert interferograms, which are simply raw data, into genuine spectra. FTIR spectroscopy is a nondestructive, structurally selective, and capable of providing spectrum information on

solid/liquid or solid/gas interfaces. The FTIR method is used to determine the infrared spectrum of transmission or absorption of a sample. The organic and inorganic constituents of the sample can be identified using FTIR. Interferometry is used by the FTIR to record information about a material placed in an IR beam. The Fourier Transform produces spectra that can be used by analysts to identify or quantify the material. The specific chemical groups that predominate in the sample will be identified using spectrum data in the automated spectroscopy software at wavelengths ranging from 600 to 4000 cm^{-1}, depending on the infrared absorption frequency range (Mohamed Shameer P. & Mohamed, 2019).

FTIR has the following benefits: it is non-destructive, precise, collects a scan every second, has greater optical throughput, and is mechanically simple.

2.8 Mechanical Properties

2.8.1 Flexural strength

Flexural strength is a material's ability to resist deformation under a bending load. The greatest stress value felt within the material at the moment of yield is expressed as a force per unit area. Bending strength can be tested in two ways: three-point and four-point bending strength tests. A three-point test involves applying a gradually increasing load in the middle of the sample until the material breaks or permanently bends. The load is applied at two points simultaneously, towards the center, for the four-point bending test, until the material breaks or permanently bends. The samples' flexural strength is the highest force observed. Flexural strength is calculated using the three-point and four-point formulas, respectively:

$$\sigma = \frac{3FL}{2wd^2} \quad \text{----------(1)}$$

Where σ = flexural strength, F= maximum force applied, L = length of the sample, w = the width of the sample, and d = depth of the sample.

2.8.2 Compressive strength

Compressive strength is the maximum uniaxial stress that a material can withstand before fracture. This test is carried out by applying equal and opposite force to the object's top and bottom. the formula for calculating compressive strength.

$$\sigma_c = \frac{F_c}{A} \text{ ----------(2)}$$

Where σ_c = compressive strength, F_c = maximum load at fracture, and A = sample area.

2.9 COMSOL Multiphysics simulations

COMSOL Multiphysics help with the analysis and simulation of complex finite element models. The software is compatible with a variety of interfaces and system configurations for partial differential equations. COMSOL provides an easy-to-use IDE that makes the work of developers in various industries much easier. The software has a unified workflow for electrical, fluid, chemical, and acoustics applications. COMSOL application builder is a great tool for creating custom simulation applications. It can be used to develop web applications or desktop applications. It is used to develop and maintain COMSOL. (COMSOL's products can help engineers achieve their goals more effectively. The software is easy to use and maintain, perfect for users who want to add complex functionality.

CHAPTER 3

Materials and Methods

3.1 Materials and Method

The materials, methods, and equipment characterization procedures utilized in the investigation are all described in depth in this chapter.

3.1.1 Materials

The materials used for conducting the research and where they were acquired can be found in Table 3.1.

Table 3.1 Materials and the location they were obtained

Materials	Location
Abonko clay	Abonko, Central Region
Coconut shells	Mallam Attah market, Accra
Palm kernel	Ashaiman market, Tema
Acacia wood	Abokobi Zimmermann gardens
Portland cement	Retail shop at East-Legon

3.2 Materials Preparation

3.2.1 Abonko clay

The Abonko clay is the most common and industrially explored secondary clay deposits in Ghana. The clay was excavated from its deposit at the Mfantseman municipality in the Central region of Ghana. All organic materials and debris were taken out from the clay and dried in the sun. The dried clay was crushed, pulverized in a jaw crusher with a mesh size of 500µm, bagged and labelled. The Abonko clay was calcined in a gas kiln found in Figure 3.1, at a rate of ~5°C/min until the required temperature (750°C) was reached and held at this temperature for 60 minutes before cooling to room temperature. A type-K thermocouple

connected to a millivolt meter is attached to the gas kiln to help monitor the temperature within the kiln.

Figure 3.1: Gas kiln for calcination

Images of the raw, pulverized, and calcined Abonko clay are shown in Figure 3.2 (a-c).

(a) (b) (c)

Figure 3.2: (a) Raw Abonko clay (b) Pulverized Abonko clay (c) Calcined Abonko clay

3.2.2 Carbonization of Coconut, Acacia, Palm kernel shells

Ten (10) kg each of coconut shells, acacia and palm kernel shells were air dried and carbonized and activated in a furnace at ~700°C at a heating rate of ~4°C per minute. The pyrolysis process took four hours for each of the biomass, with a yield ratio of 47%, 30% and

42% for the coconut shells, Acacia wood and palm kernel shells respectively. The carbonized materials were sieved through a 1 cm x 1 cm mesh. Figure 3.3 (a) to (f) shows the transformation of the agrowaste (coconut, acacia and palm kernel).

(a)

(b)

(c)

(d)

(e)

(f)

(g) (h)

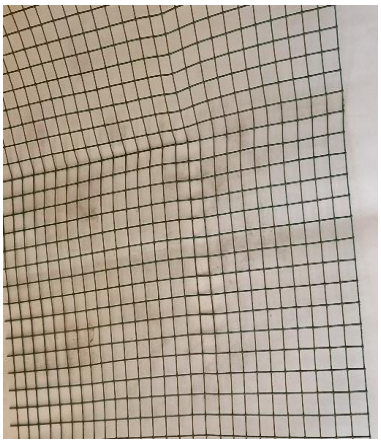

Figure 3.3: (a) Coconut shells (b) Carbonized Coconut shells (c) Acacia wood (d) Carbonized Acacia wood (e) Palm kernel shells (f) Carbonized Palm kernel shells (g) Carbonization and Activation carbon plant (h) Mesh

3.3 Composite Preparation and Batch Formulation

The calcined Abonko clay, portland cement (32.5 R), carbonized agro waste char (coconut shell, palm kernel, and acacia wood) were used in composite formation. The clay was calcined to thermally activate to react with Portland cement during hydration (Hallar-kallai, 2006), cement as the original binder and the carbonized materials to aid in thermal energy harvesting (Gonzalez et al., 2013 & Khiari et al., 2019). In Table 3.2 and 3.3 presents the batch formulations for the cubes and rectangular bars fabricated for testing. It is important to note that three different carbonized materials were used and hence, a total of thirteen compositions were made. The first composition served as the control sample which was without carbonized materials and the other twelve (12) were with varying percentages of carbonized materials. Kazmi et al., 2016 work done on other agro-waste material influenced my choice of the percentage ratio of the carbonized materials. The ratio of calcined clay to cement was 4:1, this follows the ASTM standard for preparing mortar. A total of 31% of water was used in the formulations.

Table 3.2: Batch formulation for cubes

Item	Control	5% Addition	10% Addition	15% Addition	20% Addition
ıed Clay (g)	150.0	150.0	150.0	150.0	150.0
Cement (g)	37. 5	37. 5	37. 5	37. 5	37. 5
Carbonized material (g)	-	7. 5	15.0	22. 5	30.0
Water (ml)	67. 5	67. 5	67. 5	67. 5	67. 5

Table 3.3: Batch formulation for rectangular bars

Item	Control	5% Addition	10% Addition	15% Addition	20% Addition
ıed Clay (g)	100.0	100.0	100.0	100.0	100.0
Cement (g)	25.0	25.0	25.0	25.0	25.0
Carbonized material (g)	-	5.0	10.0	15.0	20.0
Water (ml)	45.0	45.0	45.0	45.0	45.0

3.3.1 Briquettes production

The various materials were weighed in accordance with the batch formulation and mixed manually until a homogenous mix was obtained before the specific amount of water was added. The mixture was transferred into the lubricated mould box of 50 mm^3 dimensions and joggled for a minute. The cast was then left to dry for 24 hours at room temperature, de-moulded and further dried in a CJ- 9053A laboratory dry oven for 24 hours. Five samples each was produced for each formulation and Figure 3.4 (a-f) shows the steps involved in the production of the cubic and rectangular bar briquettes. The rectangular bars were fabricated using the same procedure described above.

(a) (b)

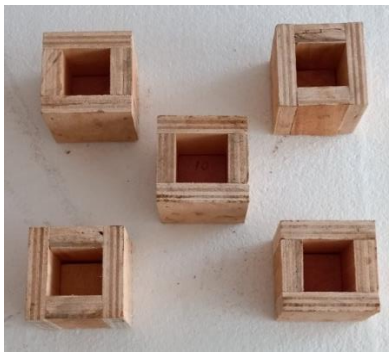

(c) (d)

(e) (f)

Figure 3.4: (a) Wooden mould (b) Mould with cast piece (c) Cast piece (d) Drying mould (e) Prism Wooden mould (f) Prism cast piece

3.4 Characterization of Samples

3.4.1 X-Ray Fluorescence

The XRF analysis was carried out at the Geological Survey Authority's chemistry laboratory using a Thermo-Fisher ARL9400 XRF system and Win XRF software for data interpretation. The analysis was performed by stimulating the samples with a primary x-ray source and measuring the resulting fluorescence emitted from the sample. The XRF analyzer was used to

establish the chemistry of the raw and calcined Abonko clays. Each element present in a sample emits a distinct set of fluorescent x-rays that are unique to that element.

3.4.2 X-Ray diffraction

The mineralogical composition of the Abonko clay, both raw and calcined was analyzed using the standard powder diffraction technique. The X-ray diffraction (XRD) analysis was conducted at the Department of Physics, University of Ghana using theta/theta geometry and operating at 35 kV and 50 mA. XRD was used to determine the crystallographic structure, different minerals/chemicals found in the clay and to identification phase of the raw and calcined Abonko clay. X-rays were incidentally irradiated into the material, and the intensities and scattering angles that left the samples were measured. To identify the phases, a continuous scan was performed from 2θ= 5.05o to 99.87° with a step size of 0.105° and a scan step time of 47.68 s. The phase analysis was carried out with using a Philips XPERT-PRO HighScore plus search software.

3.4.3 Fourier transform infrared spectroscopy (FTIR)

The Bruker Opus- 7.5.18 (Bruker, France) FTIR in the Department of Materials Science and Engineering, University of Ghana was used to analyze the test samples. An infrared radiation was passed through the samples, with some of it being absorbed and some being transmitted. The resulting spectrum represents the sample's molecular absorption and transmission, forming a molecular fingerprint. FTIR measurements were performed in the transmittance mode with a scan range of 400 – 4000 cm^{-1} using 16 scans. The data obtained from the experiments was plotted into a transmittance spectrum using Origin software. Chapter four shows the images that were obtained from the analysis.

3.4.4 Thermal Analysis of Samples

The heat content and thermal degradation analyses were performed using the SDT Q600 V20.9

Build 20 thermogravimetric and differential scanning calorimetric (TGA-DSC) system at the Department of Materials Science and Engineering, University of Ghana. 5 – 10 mg of each specimen was placed in an alumina (Al_2O_3) crucible and exposed to a direct heating ramp at a rate of 10°C/min from 20°C and 900°C using nitrogen as the purging gas. The weight-loss and heat content as a function of temperature was recorded and the data plotted using origin graphing software. The TGA-DSC system used in the study is shown in Figure 3.6.

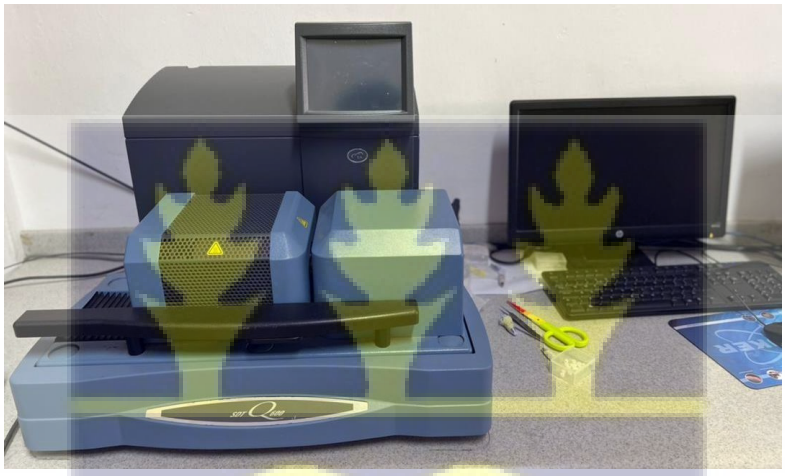

Figure 3.5: TGA/DSC SDT Q600 V20 build 20 machine

3.5 Surface morphology and phase segregation of test samples

The surface morphology, phase separation and texture of the samples were investigated using a focused beam of electrons directed at the sample to produce a complex, high magnification image of the sample's surface topography. A compound AmScope microscope with MD 130 lens was used to observe the morphological properties of the composites. The MD 130 eye piece lens have a maximum resolution of 1280 X 1024 and 1.3 MP live colour image and the 2-objective eye pieces have a magnification of WF 10X/20. The lens was attached to the trinocular port on the microscope to aid in transferring image to the camera for viewing on the computer monitor. The following steps were taken in operating the microscope:

The camera was attached to the trinocular port and connected to a computer and the microscope was turned on. The specimen for analyses was placed directly over the circle of light. While operating the microscope, the light intensity was adjusted appropriately to achieve the quality images. It is important to note that low intensity light allowed for more details to be visible and high intensity light gives a washed-out appearance.

The reflective mode analysis was carried out on the specimen with the help of the coarse and fine focus knob, which fine tunes the image for a capture.

(a) **(b)**

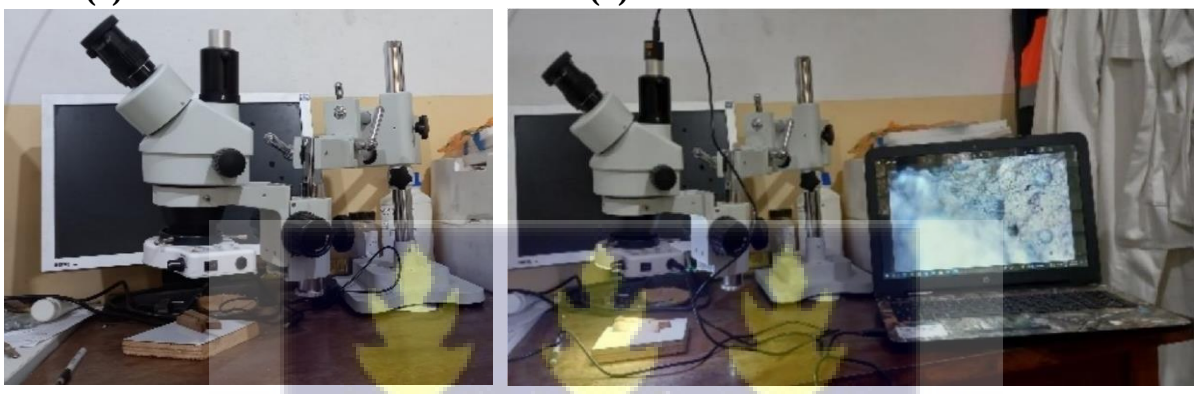

Figure 3.6: AmScope MD 130 microscope (b) Microscopy setup

3.6 Mechanical Testing of samples

3.6.1 Compressive Strength

The mechanical strength characteristics of the samples were determined by measuring the compressive strength and modulus of rupture (flexural strength). The oven dried briquettes without visible fissures were used for the compressive strength test. The dimensions of the samples were taken with a digital Vernier caliper, placed on the hydraulic press and loaded gradually until the sample fractured. Figure 3.7 (a-b) gives a pictorial representation of the process. The force applied and displacements were recorded to determine the compressive strengths. The process was carried out following BS EN 196-1:2016 standard.

3.6.2 Flexural Strength

The flexural strength was done according to the ASTM D790 (2003a) standard. The width and depth of the prism bars as well as the length of the span was taken with the help of a

digital caliper and recorded. The bar was positioned exactly at the middle of the rollers of the equipment, and the parameters input using the MOR/5-TS system. The load was applied and the load that fractured the sample is recorded, and the bending strength is calculated. Figure 3.8 (c-d) shows the MOR machine and a rectangular bar that has been tested.

(a)

(b)

(c)

(d)

(e)

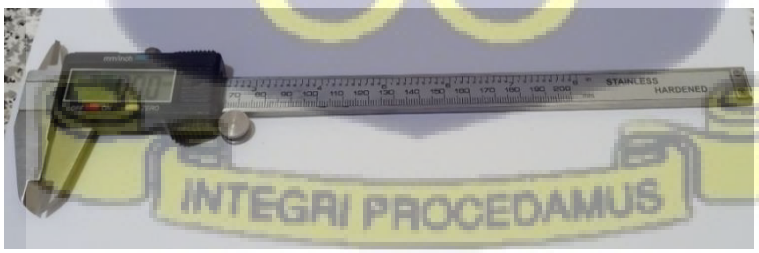

Figure 3.7: (a) Hydraulic press (b) Tested cubes (c) MOR/5-TS machine (d) Tested MOR bar (e) Digital calliper

3.7 Analytical and Finite Element Modelling

To better comprehend the interplay between the loads applied and the different agrowaste charcalcined clay test materials, finite element modelling (FEM) using the COMSOL Multiphysics software. Meshing was done using a four-node elemental mesh and ensured fine meshes were used in areas where high load interaction was perceived. To ensure a stable simulation the top and bottom boundaries were fixed, and uniform load was applied to the mid- section. The stress distribution of the steel material was estimated using the von Mises stress yielding criterion. Heat transfer mechanism was also modeled for this study a steel material with low carbon content was used together with the elastic properties as shown in Table 1.

CHAPTER 4

RESULTS AND DISCUSSION

4.1 Chemical and Mineralogical composition of clay

4.1.1 XRF Analysis of clay

The chemical analysis results in Table 4.1 show that both the raw and calcined Abonko clay mineralogical is composed of kaolinite clay rich in quartz and has a high content of iron oxide and enough potassium and titanium oxide. The major oxides present in the clay are SiO_2 (45%) and Al_2O_3 (31%) and the minor oxides identified include K_2O, NaO, CaO, TiO_2, MnO, Fe_2O_3, P_2O_5 and SO_3. The LOI was about 16%. For the calcined clay, the major oxides identified were also SiO_2 (65%) and Al_2O_3 (21%) whereas the minor oxides contents range between 0.01 – 7%.

The calcination of the clay indicated a significant percentage increase and decreases in the SiO_2 and Al_2O_3 respectively. SiO_2 increased by 40% while the Al_2O_3 decreased by 10%. The reason for this could be attributed to the calcination temperature of 750°C, which confirms the findings of Fernandez et al. and Bediako et al on the behaviour of kaolinite clays calcined above 600 °C. The presence of fluxing agents such as iron, titanium, magnesium, and potassium oxides in the Abonko clay will also aid in melting and forming a glassy phase that will improve the mechanical properties of the calcined clay.

One prominent component from the table 4.1 is the LOI of the raw and calcined clay. The reason for the difference is due to removal of organic matter due to calcination.

Table 4.1: XRF Analysis of raw and calcined Abonko clay

Oxides	Raw Abonko Clay (%)	Calcined Abonko Clay (%)
SiO_2	45.35	64.74
Al_2O_3	30.90	20.82
K_2O	0.62	1.24
NaO	0.75	1.38

CaO	0.07	0.01
TiO_2	0.64	0.78
MnO	0.02	0.05
Fe_2O_3	4.94	7.03
P_2O_5	0.02	0.00
SO_3	0.22	0.11
LOI	16.47	-
Total	**100**	**96.16**

4.1.2 XRD Analysis of clay

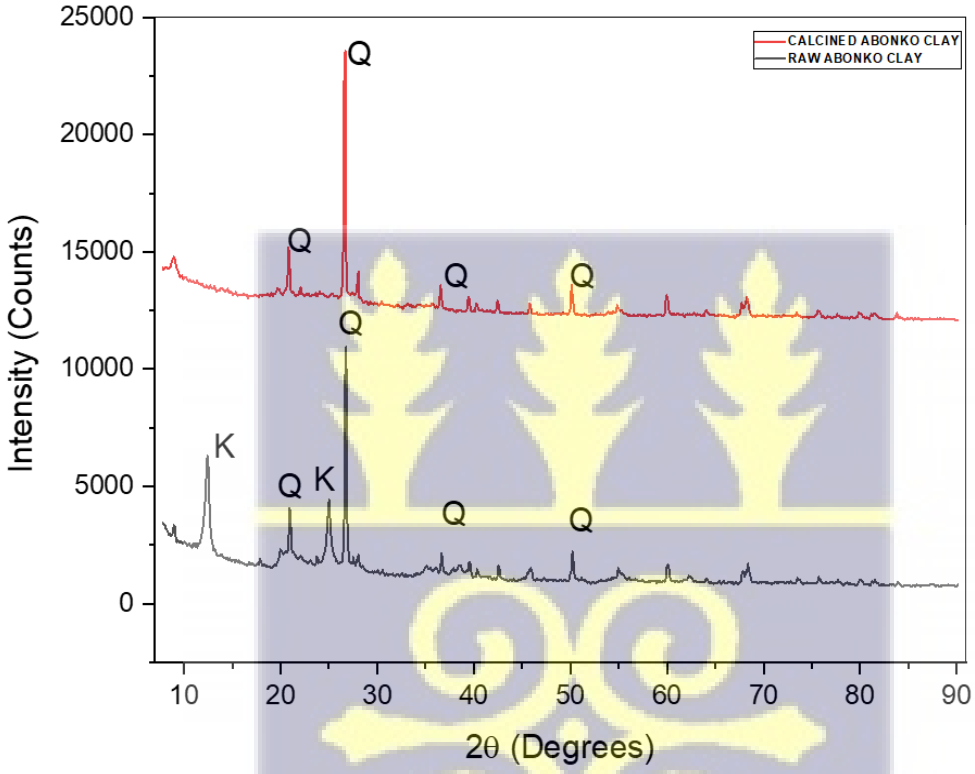

Figure 4.1: XRD Results for raw and calcined Abonko clay

The XRD analysis report in Figure 4.1 shows the crystallography structure and the phases present in the raw Abonko clay and Abonko clay calcined at 750°C. Both clays have two distinct patterns present, that is Kaolinite ($Al_2O_3.2SiO_2.2H_2O$) and quartz (SiO2). Similar peaks position and intensities for the quartz phases was observed in the raw and calcined clay, but there were difference in the kaolinite peaks. The calcining of the clay at 750°C had a massive effect on the kaolinite phase in the raw Abonko clay, several kaolinite peaks

disappeared while the intensity of others reduced considerably. This is confirmed by Von-Kiti et al. (2016) who reports that existing kaolinite peaks or reflection at (010) and (020) are loss when Wassa kaolin is calcined. However, Akolekar (1997) and Kovo (2011) in their study reported that quartz peaks in the calcined clay (metakaolin) were present but with reduced intensities. Figure 4.1 depicts an XRD analysis of the raw and calcined Abonko clay.

4.2 FTIR Analysis

4.2.1 Control samples

The FTIR plot for the control (composite made with calcined clay and cement) is presented in Figure 4.2a. The characterization was carried out between 400- 4000cm-^{1}. The results shows that about 10 peaks are present, indicating that it is an organic material. A strong band was observed at 3398 cm-^{1}, however there are no prominent peaks between 2350 -3380 cm-1. A few peaks with variable intensities were observed in the following 2324 – 428 cm^{-1} region. These included 2324, 2107, 1981, 1423, 1010, 874, 716, 673, 592, and 428 cm^{-1}.

The material has single, double, and triple bonds. The two C≡C triple bond detected between 2100 – 2324 cm-^{1} in the material indicates the existence of hydroxyl (-OH), and a hydrogen bond is detected at 3397 cm-^{1}. This hydrogen bond indicates the presence of a natural hydrous silicate in the composite (Lee, Kim, & Moon, 2003). The hydroxyl compound is followed by the presence of spectra at frequencies of 1600-600 cm-^{1}.

4.2.2 Palm kernel char-Calcined Clay-Cement Composite

Figure 4.2b represents the FTIR results of the palm kernel char composite. The figure shows vibration bands occurring at 428, 777, 1028, 1428, 2060, 2192 and 3373 cm-^{1}. Vibration bands occurring at such points corresponds to C-H, C=C, C-O, C-H, C=O, C≡C and O-H.

The FTIR analysis of the palm kernel-clay composite shows the presence of seven peaks. These peaks present are single, double or triple bonds in the material. The C≡C triple bond at 2182 cm-^{1} in the composite signifies the presence of hydroxyl (O-H). A hydrogen bond is

detected at 3373 cm-^{1} this signifies the presence of natural hydrous silicate (Lee, Kim, & Moon, 2003) and this follows with research done by Bediako et al. that vibration bands at 3373 cm-^{1} conform to a metal bonded to a hydroxide group. There are two double bonds existing in the composite, the C=C bond at 777cm-^{1} is a crystalline structure of the cellulose representing the presence of char in the composite, and the C=O bond at 2060 cm-^{1} indicates the presence of bonds in carbonate anion (Xu, Yu, Tesso, Dowell, & Wang, 2013). The C-O bond detected at 1028 cm-^{1} signifies a cellulose bond (Fackler, et al., 2011). The FTIR results for the palm kernel composite are found in Figure 4.2 (b).

4.2.3 Coconut char-Calcined clay-Cement Composite

The FTIR plot of the coconut char composite in Figure 4.2c. The characterization was carried out between 400 and 4000 cm-^{1}. The Analysis results of the coconut composite show the presence of three single bonds, a double bond, and a triple bond. The single bonds C-H, C-O are bonds in cellulose as observed by Xu et al,. (2013) and a O-H bond is a natural hydrous silicate as reported by Lee et al., (2003). The vibrations bands of the single bonds were detected at 428 cm-^{1}, 1010 cm-^{1} and 3349 cm-^{1}, respectively. The C=C bond detected at 776 cm-^{1} is a hexagonal charcoal form, confirming char's presence in the composite. The triple bond at 2081 cm-^{1} affirms the hydroxyl (O-H) hydrogen bond at 3349 cm-^{1} is a hydrous silicate Lee et al., (2003).

4.2.4 Acacia char-Calcined clay-Cement Composite

The FTIR analysis of the acacia composite can be found in Figure 4.2 (d). The composite is characterized by a strong band at 3374 cm-1 which is a O-H bond representing natural hydrous silicate (Lee et al., 20003), while several peaks with variable intensities were observed at 2324, 2050, 1981, 1416, 1010, 874, 775 and 428 cm-1. The vibrations bands at 1416 - 874 belong to stretching and bending vibration of C-H and C-O bonds in cellulose (Xu et al., 2013 and Fackler et al., 2011).

(a)

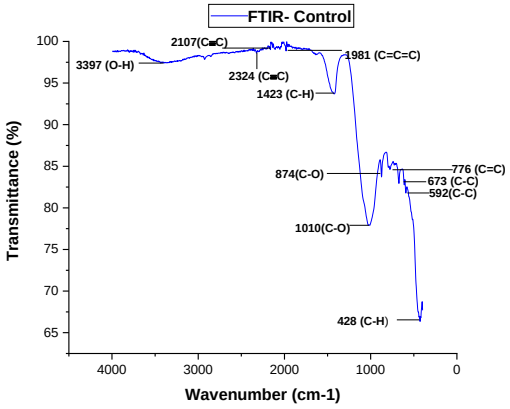

(b)

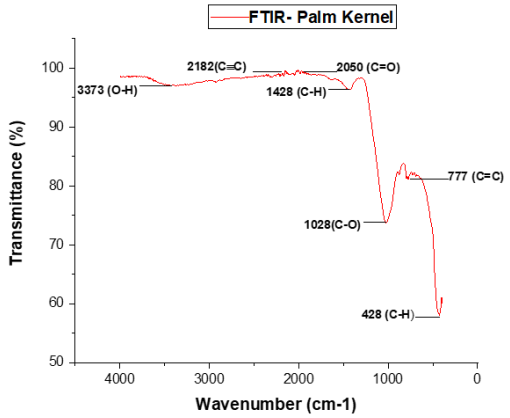

(c)

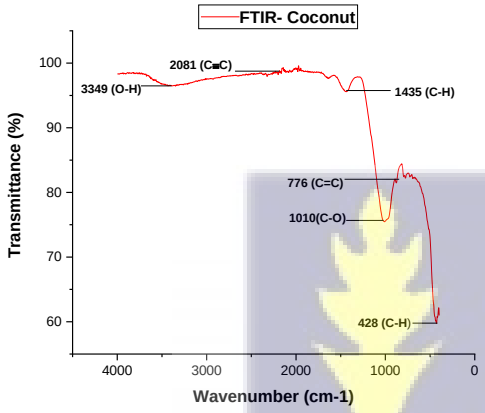

(d)

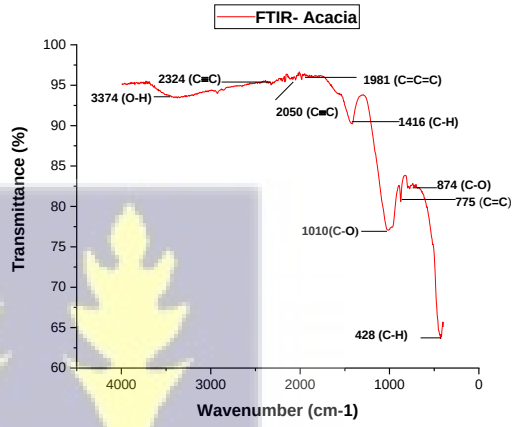

Figure 4.2: FTIR Results of (a Control composite (b) Palm kernel char composite (c) Coconut shell char composite (d) Acacia char composite

4.3 Mechanical Properties

4.3.1 Compressive strength

4.3.1.1 Palm kernel char-Calcined Clay-Cement Composite and Control

The compressive strength result recorded for the control sample is 7.61N/mm^2, and this is above the 3.5 N/mm^2 minimum required compressive strength of bricks for construction. From the graph in Figure 4.3(a), it can be deduced that the control sample recorded a higher compressive strength than all the palm kernel composites, that is, 5%, 10%, 15% and 20% addition. For 5%, 10%, 15%, and 20% addition, the compressive strength of the palm kernel samples was 4.60, 4.23, 4.14, and 3.03 N/mm^2, respectively. The results show that the 5%

addition had the highest compressive strength: however, as the char increases, the compressive strength decreases. The decrease in compressive strength is attributed to the increased char's high defect area in the matrix (Dayananda, KerthiGowda, & Easwara Prasad, 2018). However, the compressive strength measured for the 5%, 10%, and 15% palm kernel composites is greater than the average compressive strength of building bricks, which is 3.5 N/mm^2. This is in accordance with ASTM standards for compressive strength of building materials.

(a) (b)

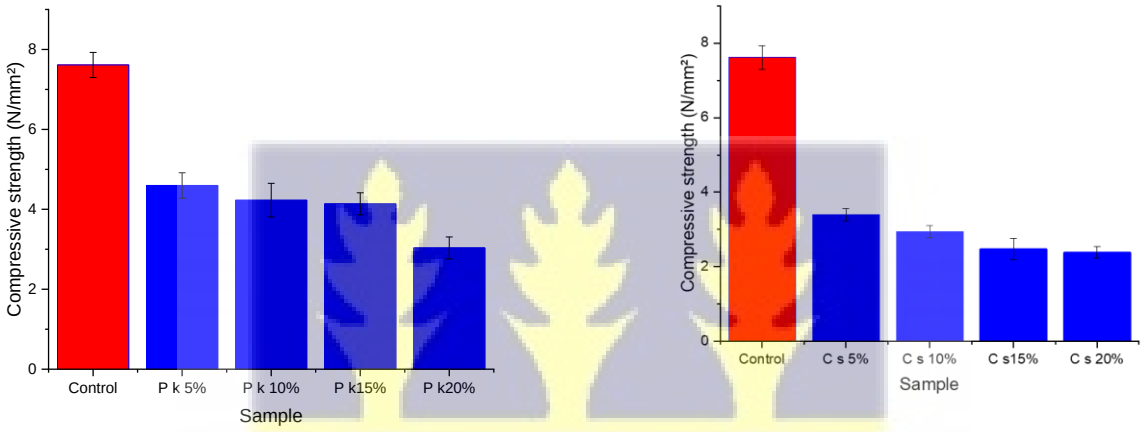

(c)

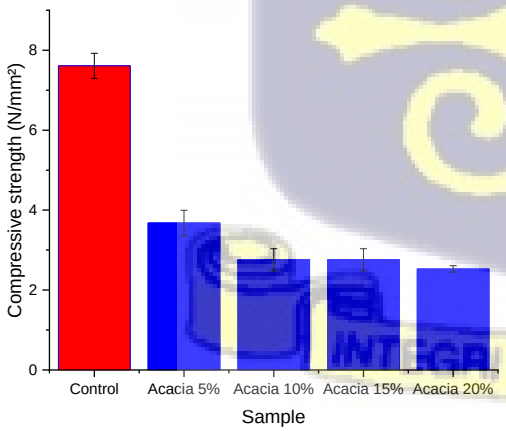

Figure 4.3: Compressive strength results for (a) Palm kernel char composite (b) Coconut shell char composite (c) Acacia char composite

4.3.1.2 Coconut shell char-Calcined Clay-Cement Composite and Control

The compressive strength of the coconut shell-clay-cement composite was 3.40 N/mm^2, 2.94 N/mm^2, 2.48 N/mm^2, and 2.39 N/mm^2 for 5%, 10%, 15%, and 20% char addition, respectively. This composite had lower compressive strength values for the minimum compressive strength required for masonry bricks. The graph in Figure 4.3(b) shows a decrease in the composite compressive strength as the char increases, which is due to an increase in defect areas in the matrix as the char increases. The compressive strength of the coconut shell composites was approximately 45% lower than the control samples.

4.3.1.3 Acacia Char-Calcined Clay-Cement Composite and Control

Figure 4.3(c) represents the compressive strength of the Acacia char-cement-clay composite; the graph shows that the control samples recorded a higher compressive strength (7.61N/mm^2) than the acacia composite. The compressive strength for 10%,15% and 20% recorded lower compressive strength values, however the 5% char addition had a compressive strength (3.53 N/mm^2) comparable to the minimum compressive strength (3.5 N/mm^2) for blocks for masonry. It can also be observed that the 10% and 15% char addition recorded the same compressive strength values. Generally, the reduction in compressive strength can be attributed to the porous nature, less strength and volume of the char content in the composite ( ). Since the char is very porous, they fracture easily when load is applied to the blocks hence the lower compressive strength.

4.3.2 Modulus of Rupture

4.3.2.1 Palm kernel shell-Calcined Clay-Cement Composite

Figure 4.4(a) represents the flexural strength of the control and palm kernel composites; according to the results, the composite with 5% palm kernel addition had the highest flexural strength of 1.04 Kg/mm^2, while the control sample had a flexural strength of 0.53 Kg/mm^2.

On the other hand, the flexural strength of the palm kernel composites decreased from 1.04 Kg/mm^2 to 0.33 Kg/mm^2; it can therefore be concluded that the volume of the palm kernel char had a significant effect on the flexural strength. In General, the palm kernel shell char composites' flexural strength decreased linearly as the char volume increased from 5%- 20%, thereby creating voids within the composites leading to weaker interfacial adhesion. This is a confirmation of what other researchers obtained in their work.

4.3.2.2 Coconut shells char-Clay-Cement Composite

The flexural strength results for the control sample, as well as the 5%, 10%, 15%, and 20% coconut shell addition composite, are shown in Figure 4.4(b). The control sample had the highest flexural strength of 0.53 Kg/mm^2, and the flexural strength of coconut shell composites decreased as the char increased. The results also show that the flexural strength (0.17 Kg/mm^2) was the same for the 10%, 15%, and 20% char additions.

4.3.2.3 Acacia char-Clay-Cement Composite

The flexural strength results of the control and acacia composites are shown in Figure 4.4(c); the results show that the control sample recorded a higher flexural strength (0.53 Kg/mm^2). It is evident from the graph that the acacia composites' flexural strength reduced marginally from 0.36 Kg/mm^2, 0.35 Kg/mm^2 and 0.31 Kg/mm^2 for the 5%, 10% &15% and 20%, respectively.

(a) (b)

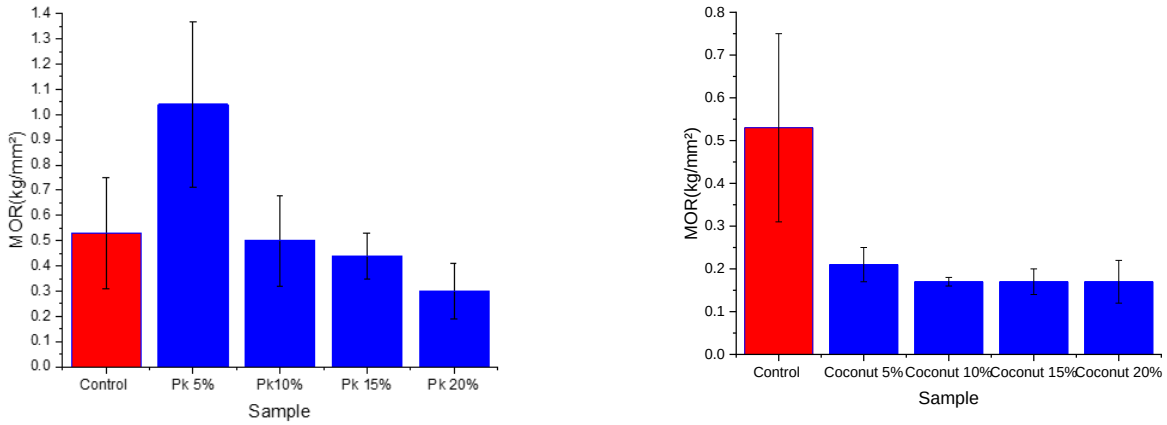

(c)

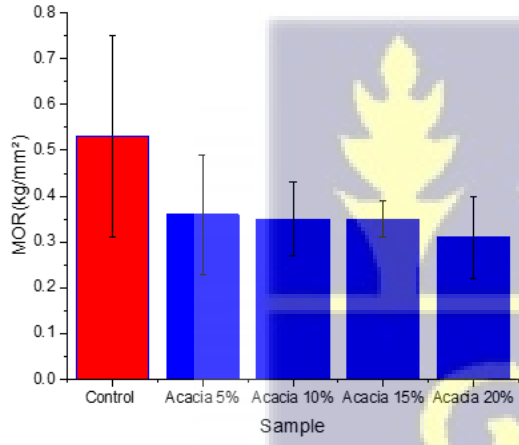

Figure 4.4: Flexural strength results for (a) Palm kernel char composite (b) Coconut shell char composite (c) Acacia Char composite

4.3.3 Thermogravemetric Analysis

4.3.3.1 Coconut char-Calcined Clay-Cement Composite

(a) (b)

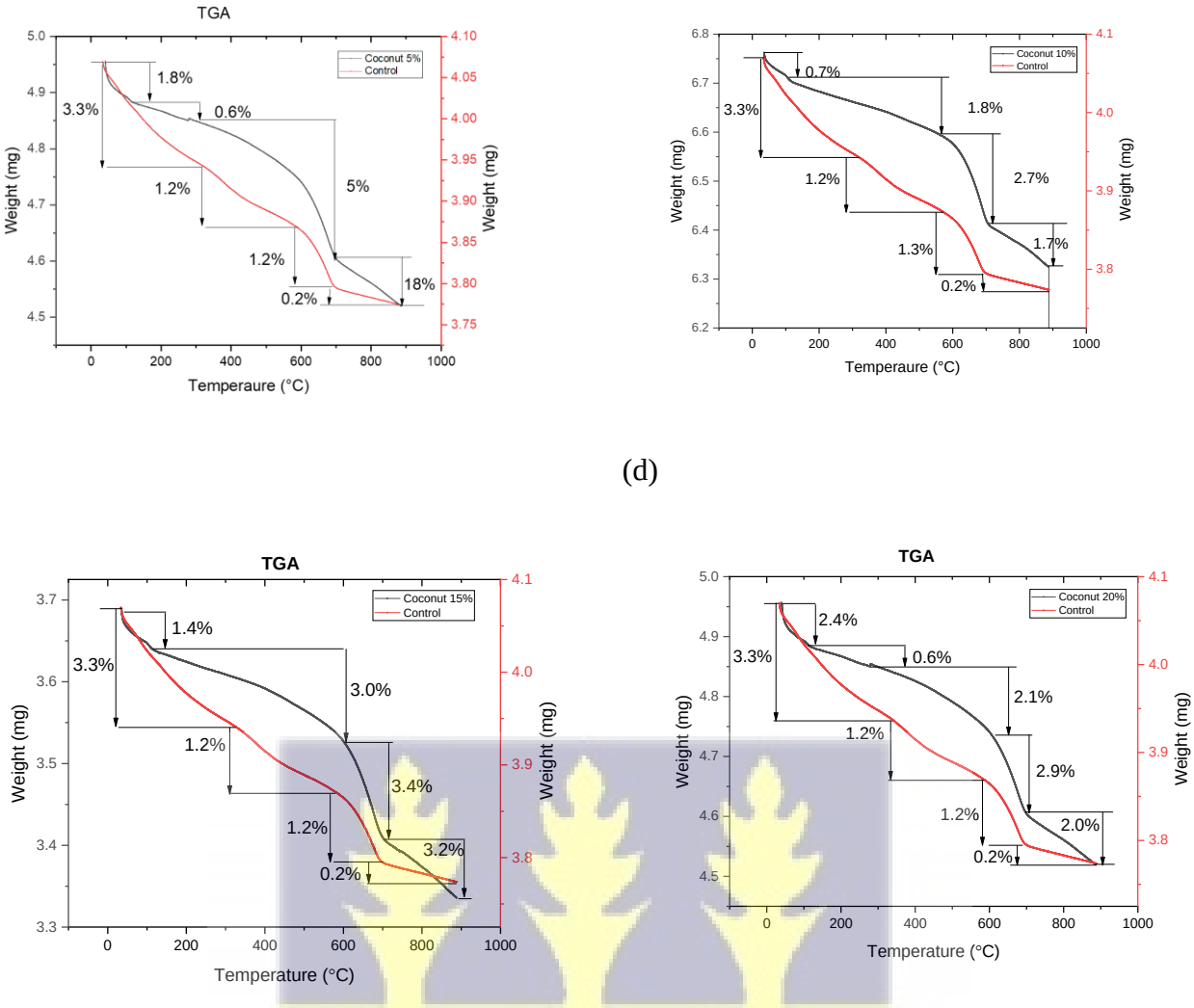

Figure 4.5: TGA results for Coconut Char composite (a) 5% Addition (b) 10% Addition (c) 15% Addition (d) 20% Addition

The weight loss of the samples as they were heated was monitored using the thermogravimetric for the control sample, palm kernel composite, coconut composite and the acacia composite described above.

According to Figure 4.5(a), the water loss of 3.3% and 1.8% begins at 39.8°C and 40 °C for the control and 5% addition of coconut char, respectively, and continues evolving up to 398°C for the control and coconut char sample, respectively, due to the breaking of chemical bonds and decomposition as temperature increases. The presence of these bonds is confirmed by FTIR analysis: C=C, C-H, O-H, and C-O. The loss of weight can be attributed to a decrease in moisture content. At 712 °C - 888 °C, the weight of the coconut composite

decreased by 5% and 18%, respectively. The 18% weight reduction can be attributed to the decomposition of lignin in the biomass, as reported by Chuan et al., and decarbonisation of calcium carbonate in the cement at 700- 900°C reported by (P.E. Grattan-Bellew, 1996). A total of 5.9% and 25.4% weight loss was recorded for the control and coconut composite respectively as it was heated to 888°C, showing that the control sample was more stable.

Figure 4.5(b) depicts the weight loss for the coconut 10% composite and the control sample; the graph shows four distinct weight losses. The removal of physical and chemical water, as well as the dehydration of the Portland cement, causes the first weight loss between 34°C 111°C and 34°C - 398°C for the coconut composite and control sample, respectively. The second weight loss observed between 111°C - 562°C and 398°C - 635°C for the coconut composite and control sample could be attributed to portlandite dehydroxylation, chemical bond breakdown, and decomposition. For the coconut composite and control samples, the third weight loss was recorded between 562°C -709°C and 635°C -783°C. The fourth weight loss was recorded between 709°C - 888°C, 783°C- 889°C for the coconut composite and control sample; there was a low weight loss of 1.7%-0.2% (at higher temperatures, a metastable state transforms from the amorphous condition into crystalline units, inhibiting calcined clay reactivity) supports by (Fernandez 2011). As a result, material stability is critical, and the graph in the figure shows that the composite and control samples had total weight losses of 6.9% and 5.9%, respectively.

Figure 4.5(c) shows the TGA result for the control sample and the 15% addition of coconut shell char. From the graph, there is an initial 1.4% weight loss for the coconut composite when the temperature was raised from room temperature to 112°C, and this change is associated with the removal of water from the composite. The second weight loss of 3% was observed between the temperatures of 112°C to 600°C, and this could be due to dehydration reactions of several hydrates in the cement and dehydroxylation of portlandite. The final

weight loss of 3.2% at temperatures ranging from 705°C to 886°C could be attributed to dehydroxylation of the clay, decarbonisation of calcium carbonate derived from the clinker, and further char breakdown. The 15% coconut char addition resulted in a total weight loss of 11%, compared to 5.9% for the control sample.

The graph in Figure 4.5(d) shows a total weight loss of 5.9% for the control and 7.1% for the composite. When the sample was heated from 34°C to 126°C with a 20% addition of coconut char, a 2.4% weight loss was observed, which can be attributed to water loss. Second, as previously reported by other researchers, the 0.6% weight change was caused by the breakdown of chemical bonds in the cement and char components. A total of 7% weight loss was observed between 277°C and 886°C, which could be attributed to the calcined clay transforming from an amorphous to crystalline state.

4.3.3.2 Palm kernel Char-Calcined Clay-Cement Composite

The graph in the Figure 4.6(a) shows the TGA results for the control sample and the 5% addition of palm kernel char composite. The results show a total weight loss of 5.9% and 6.2% for the controlled and palm kernel composite showing that these composite materials are thermally stable. The first stage of weight loss of 0.9% was recorded between the 34°C-323°C, and this is due to loss of water and the dehydration of the cement. The second stage took place between 324°C and 509°C and was caused by the dehydroxylation of portlandite, another hydration product. Between 510°C and 707°C, calcium carbonate from the cement begins to decarbonise, resulting in a 3.1% weight loss. The final weight loss of ~ 0.9% occurred between 708°C and 888°C due to the clay dehydroxylation as well as decomposition of the carbon phase of the char. (A. Nyamful et al., 2020).

The TGA results of the 10% addition of palm kernel char in Figure 4.6(b) reveal four distinct processes. The first two processes represent evaporation of adsorbed water and cement dehydration, which occurred between 35°C and 364°C and accounted for 1.8% weight loss.

At 365°C-705°C, a further weight loss of 4.6% was observed, which can be attributed to the cement. The final process resulted in a 0.9% weight loss, which could be believed to be due to dehydroxylation of the calcined clay, carbon decomposition in the char, and calcium carbonate decarbonisation. From the graph, a total weight loss of 5.9% and 7.3% was witnessed in the control sample and 10% palm kernel char addition, respectively.

Figure 4.6(c) presents the TGA results of the control and 15% addition of palm kernel composites, showing that four different processes occurred. The palm kernel composite material lost 2.5% weight in the first two stages due to evaporation of adsorbed water and dehydration of the cement, which occurred between 35°C and 356°C. However, there was a high weight loss of 8% at the third stage occurring between 356°C -709°C due to the decomposition of the carbon phase and dehydroxylation of portlandite. The final stage had a weight loss of 1.1% between 710°C and 888°C due to calcined clay dehydroxylation and calcium carbonate decarbonisation. The composite lost 10.4% of its total weight.

Figure 4.6(d) depicts the results of the TGA analysis of the control samples and the addition of 20% palm kernel char; the graph shows four processes that occurred when the samples were heated from room temperature to 900°C. For the palm kernel sample, a weight difference of 1.5% was recorded when the sample was heated from 35°C to 118°C due to the water's evaporation. The second process occurred between 119°C to 358°C, which led to a 1.5% reduction in the weight of the sample; this could be due to the dehydration of the cement in the composite, between 359°C and 709°C, carbon from the char begun to decompose leading to a significant weight loss of 8% especially since this composite had many chars. The final process recorded 1.5% weight loss, between 710°C to 886°C. The increase in temperature above the calcination temperature of the clay led to the dehydroxylation of clay and the decarbonization of calcium carbonate from the cement.

(a) (b)

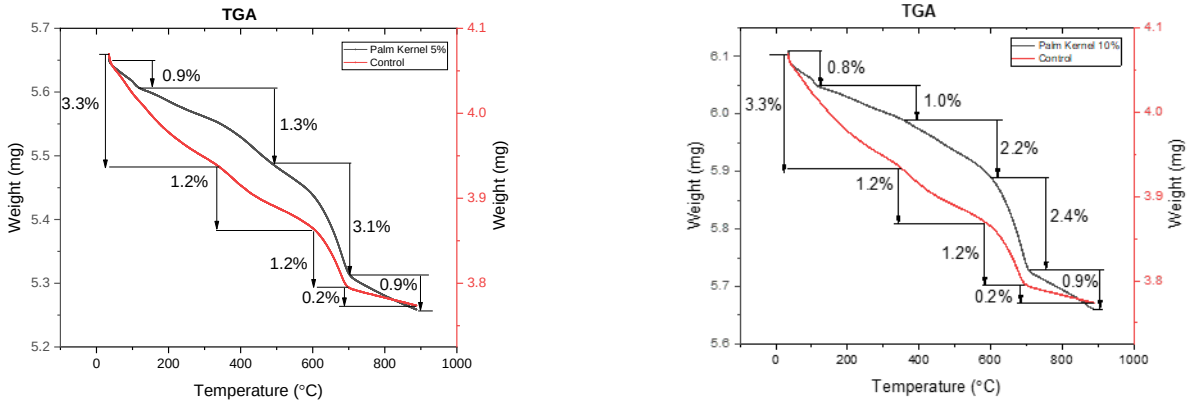

(c) (d)

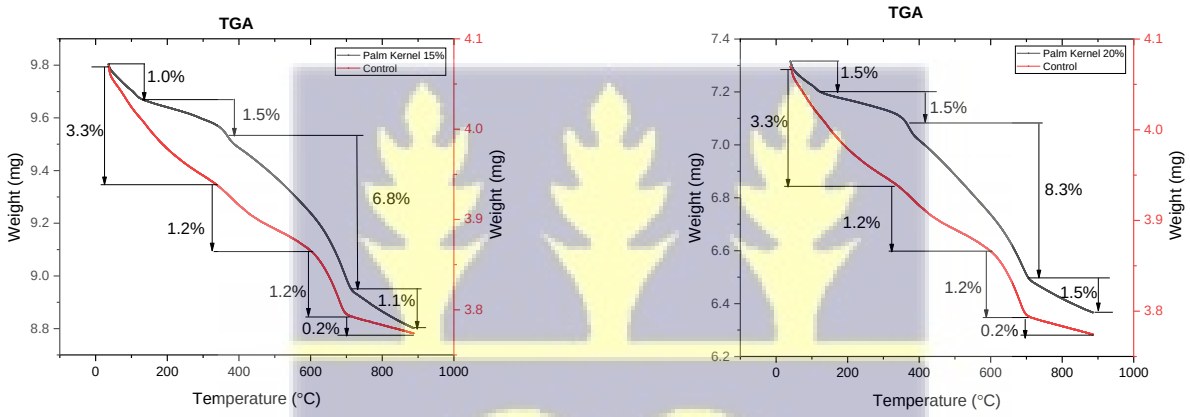

Figure 4.6: TGA Results for Palm kernel Char composite (a) 5% Addition (b) 10% Addition (c) 15% Addition (d) 20% Addition

4.3.3.3 Acacia Char- Calcined Clay Composite

The TGA results for the 5% addition of acacia char composite and the control sample can be found in the graph in Figure 4.7(a). It is evident from the graph that five distinctive processes occurred when the acacia composite was heated from room temperature to 900°C, and this led to a 5% weight loss that is from 5.10mg to 4.83mg. However, the control sample had a total weight loss of 5.9% that is from 4.07mg to 3.77mg; this shows that the acacia sample is more stable than the control sample even though decomposition of carbon occurred in the

acacia composite between 699°C-831°C. The weight loss in the composites can be attributed to water evaporation, decomposition of char (carbon), decomposition of calcium carbonate and dehydroxylation of clay. The TGA analysis results in Figure 4.7 (b) show 5.9% weight loss for the control sample and

7.9% weight loss for the 10% acacia char addition, making the control sample more stable. From the graph, it can be observed that between 35°C- 635°C, the control sample lost more weight than the acacia sample that is 4.5% and 3.9%, respectively; however, at higher temperatures, it was vice versa due to the decomposition of char in the acacia sample. Figure 4.7(c) shows the TGA analysis results for the control and 15% acacia char addition. The results show that the control sample had a more rapid weight loss from the onset than the acacia sample. However, as the temperature increased, the acacia sample began to lose weight due to the carbon decomposition in the sample. This occurred in the third process of the acacia sample, between 587°C- 650°C. Overall the control sample had a total weight loss of 5.9% and 8.6% for the acacia sample. The TGA analysis results in Figure 4.7(d) show the behaviour of the control sample and the 20% acacia char sample when it is heated, and it determines both the temperatures at which the materials lose weight and the exact weight losses. From the results, the control sample's initial weight of 4.07 mg was reduced to 3.77 mg after it was heated to 900°C, which is 5.9%, and the acacia sample from 6.17 mg to 5.57 mg, which is 10.5% weight loss. It can also be seen that most of the weight loss occurred between 400°C-888°C amounting to 7.3% of the total weight loss, largely due to the decomposition of carbon.

(a)

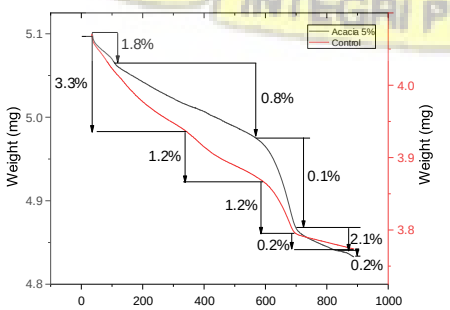

(b)

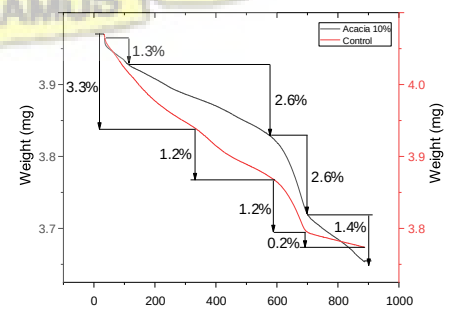

(c) (d)

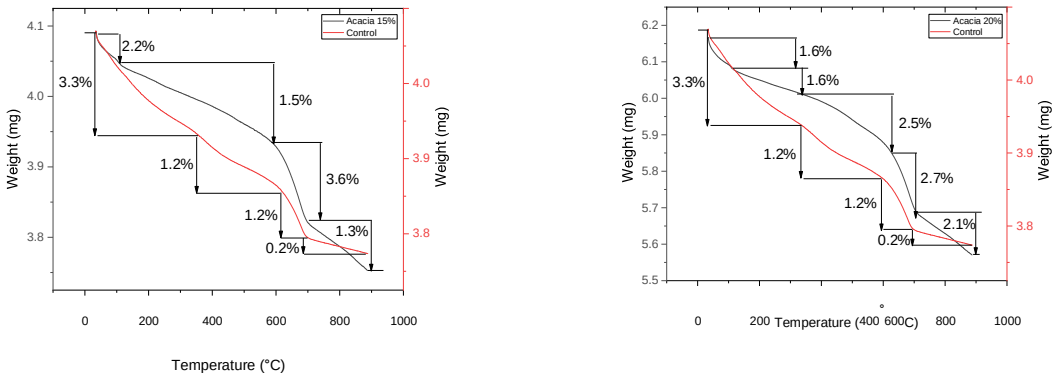

Figure 4.7: TGA Results for Acacia Char composite (a) 5% Addition (b) 10% Addition (c) 15% Addition (d) 20% Addition

4.3.4 Differential Scanning Calorimetry

4.3.4.1 Control sample

The DSC results provide data on the ideal behaviour of the material as it is heated and Figure 4.8 shows the thermal behaviour of the control sample. At about 200°C and 395°C an exothermic reaction occurred, and this can be associated to crystallization. Above 410°C the sample begun to absorb heat which may be due to change in the amorphous material and that accounts for the high percent of weight loss between 400°C-900°C. It is interesting to note that around 680°C another endothermic reaction took place, and this may be due to glass transition. At 900 °C the sample was absorbing -14 mW heat.

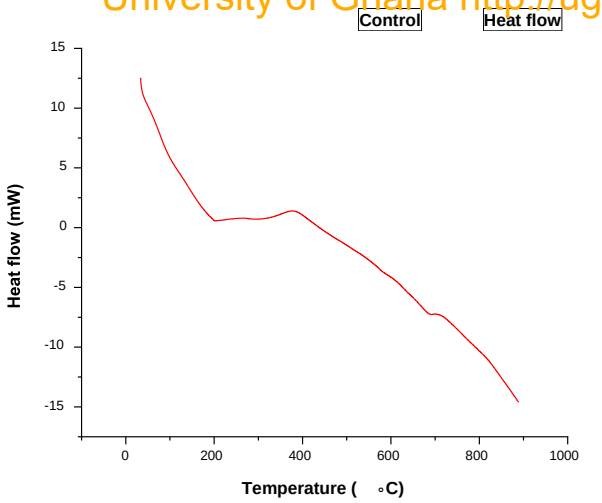

Figure 4.8: DSC Results for Control sample

4.3.4.2 Palm kernel Char-Calcined Clay-Cement Composite

Figure 4.8(a) shows the heat release with respect to the weight loss of the 5% palm kernel char composite, the results show an exothermic reaction at 200°C and an endothermic reaction around 520°C to 900°C. From the graph, it can be observed that from 520°C heat flowed into the sample, and this can be linked to an endothermic glass transition. The TGA results of 5.3% weight loss that occurred across 520°C to 900°C confirms this reaction.

The exothermic reaction that occurred at 200°C can be attributed to crystallization. Endothermic reaction occurs from 500°C - 900°C, around 720° C the reaction led to heat absorption of 20mW. The total heat flow recorded was between 11mW to -42mW. The results of the TGA for the 10% char addition are represented in Figure 4.8(b).

15% Palm kernel char composite had heat flow between 15 mW to -42 mW from room temperature to 900°C. The heat absorbed or released into the sample was due to various reactions or transformation taken place due to an increase in temperature. From the graph above, we observed an exothermic reaction around 200°C which ends around 510°C and endothermic reactions between 520°C- 900°C. From the TGA results, we observe weight loss of 7.9% between 357°C-900°C and this can be attributed to the endothermic reaction that occurred.

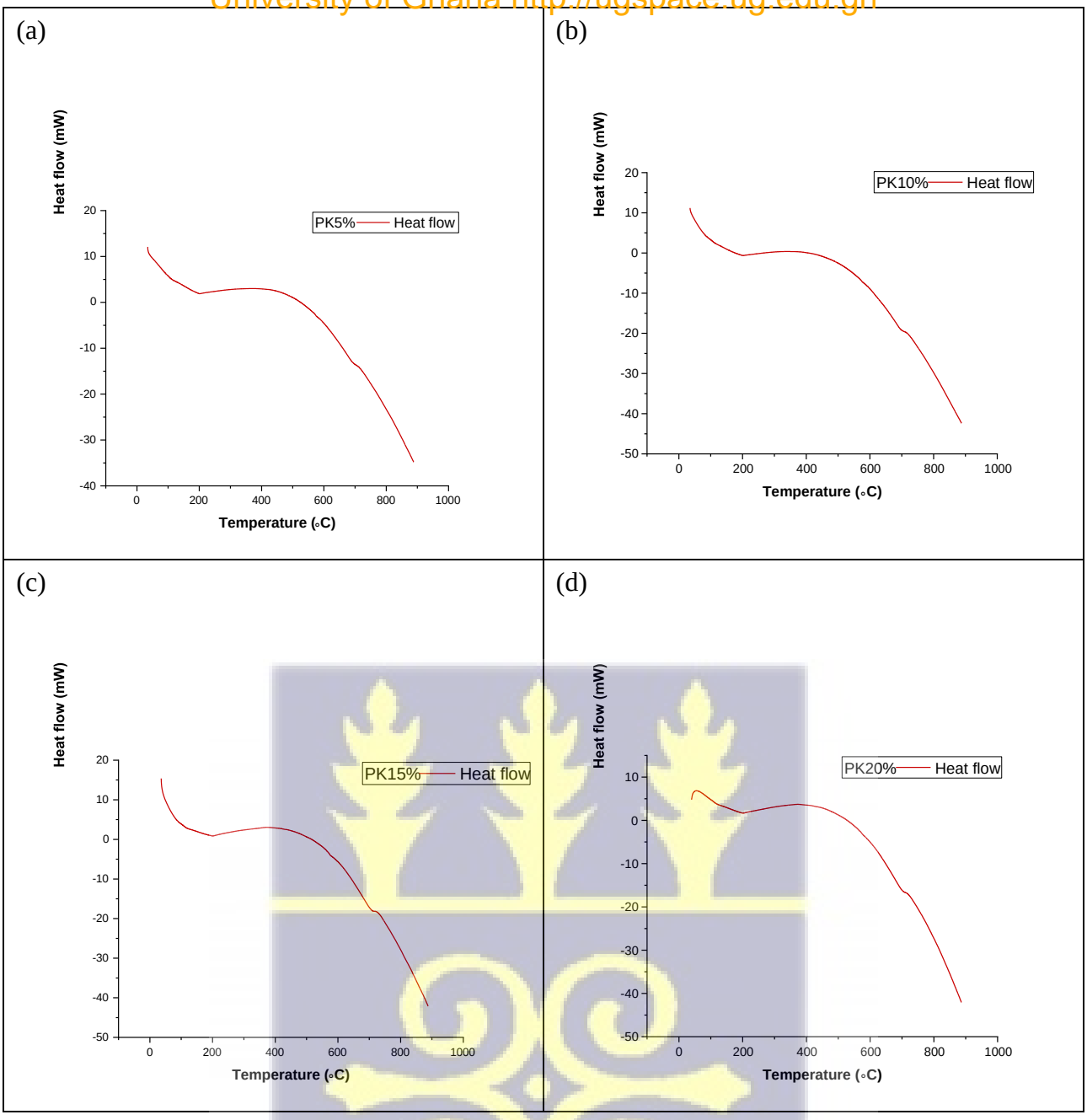

Figure 4.9: DSC Results for the Palm kernel Char composite (a) 5% Addition (b) 10% Addition (c) 15% Addition (d) 20% Addition

4.3.4.3 Coconut Char-Calcined Clay-Cement Composite

The DSC characteristics of coconut char 5% composite is represented pictorially in Figure 4.10(a). From the graph we observe both an exothermic and endothermic reaction. The composite material began to release heat immediately heat was introduced into the system and this continued until 599˚C. It is also noted from the graph that heat released from the

system reduced until about 210˚C when the amount of heat released begun to increase. This continued to 500˚C when before reducing. An endothermic reaction occurred between 600°C-900°C, this could be due desorption, melting breakdown reaction or a change in crystal structure.

Figure 4.10(b) is a DSC graphical representation of 10% coconut char composite: the results show an exothermic reaction from 35˚C to 503°C, and an endothermic reaction from 505°C to 900°C. The corresponding weight loss can be found in the TGA results. From the graph, it can be observed that from 505°C heat flowed into the sample, and this can be linked to an endothermic glass transition or a change in crystal structure. The TGA results of 4.5% weight loss that occurred across 505°C to 900°C confirm this reaction.

The DSC results in Figure 4.10(c) provide data on the ideal behaviour of the 15% coconut char composite material as it is heated. Just like the other coconut char composite, there is an initial heat flow out of the sample when the temperature rises from room temperature to 549˚C representing heat flow energy of 10 m/W to0.01 m/W. At temperatures between 550°C to 888°C, an endothermic reaction representing heat absorbing energy of -2.9 E to -33 m/W. The exothermic and endothermic reactions were due to a change in crystal structure.

The DSC results in Figure 4.10(d) represent information on change in heat flow rate and heats of transition of 20% coconut char composite. The graph shows an initial heat released out of the sample when the temperature was raised from 40˚C to 475˚C and heat absorption as the temperature further increases to 888˚C the change in heat flow from exothermic to endothermic reaction was due to a change in crystal structure. The accompanying weight loss of these reactions is established in the TGA results. The overall heat flow recorded was 0.5 m/W to 37 m/W.

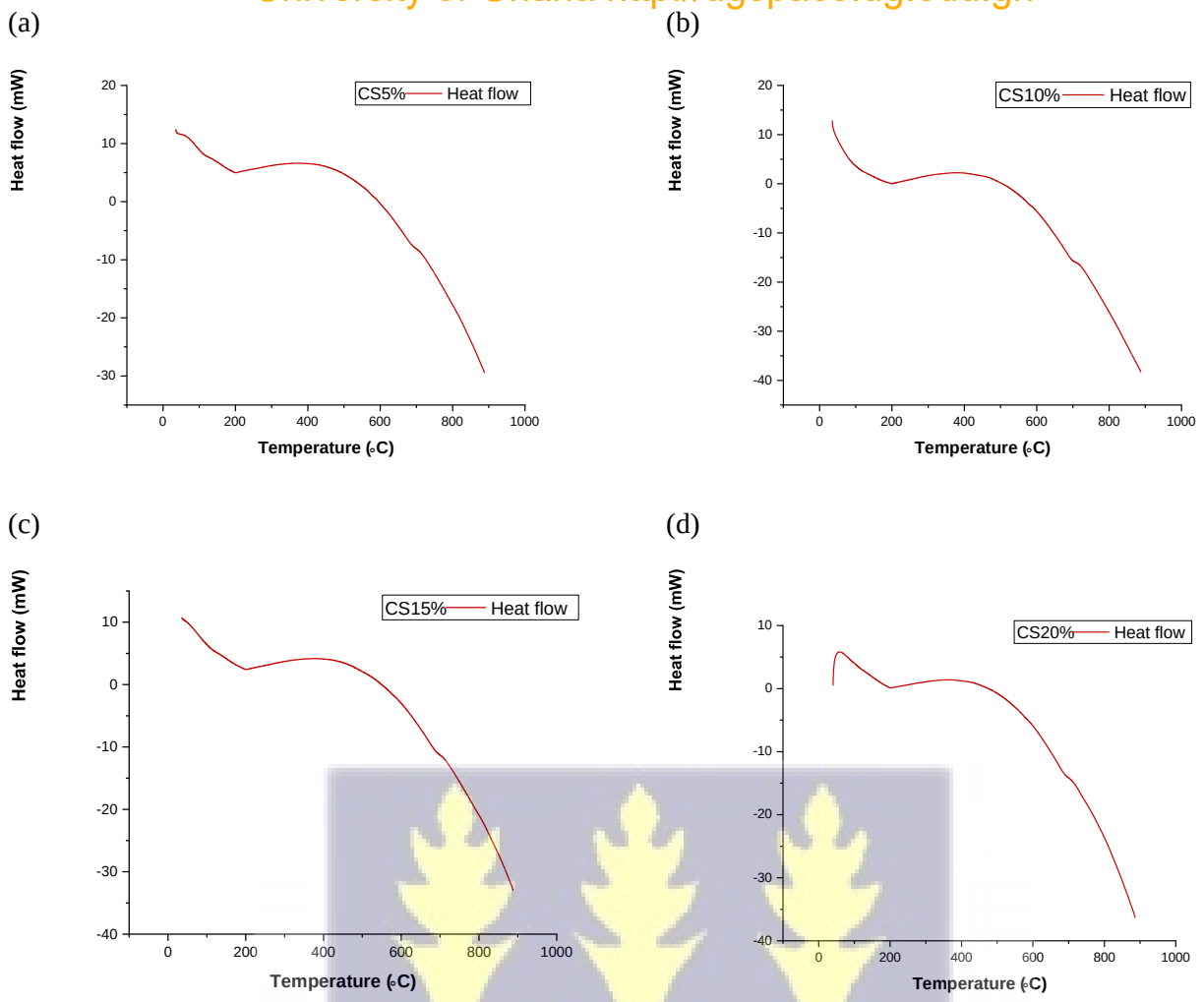

Figure 4.10: DSC Results for Coconut shell Char composite (a) 5% Addition (b) 10% Addition (c) 15% Addition (d) 20% Addition

4.3.4.4 Acacia Char-Calcined Clay-Cement Composite

From Figure 4.11(a) we observe a downward trend of heat been released from the sample till 128°C when the sample began to experience an endothermic reaction. Between 128°C to 210°C, heat absorbed by the sample was rapid, however above 210°C heat been absorbed into the sample increased steadily until about 500°C. Beyond that, the sample began to absorb heat more rapidly. The rapid absorbing of heat can be related to the energy required for a phase change in the sample.

Upon the introduction of heat to the sample, we detect heat released of 12.2 mW at 35°C, however as the temperature increased the heat been released reduced steadily. The steady reduction in the exothermic reaction continued to 285°C then the heat released begun to increase again till 325°C. The heat released from the sample may be due to confirmational energy because molecules are arranging themselves or due to chemical reaction. At 420°C, an endothermic reaction occurred and continued till 888°C. From the DSC result in Figure 4.11(b), we notice that the sample absorbed more heat as the temperature increased from 450°C to 888°C. Heat flowing into the sample leads to glass transition which causes a change in size as established from the TGA results that is 6.8% weight loss around the said temperature.

From Figure 4.11(c) we observe a downward trend of heat released from the sample till 195°C when the sample began to experience an endothermic reaction. Between 196°C to about 900°C, the sample began to absorbed heat. This endothermic reaction was steady until about 685°C, above 685°C, the rate at which heat was being absorbed reverted. The rapid absorbing of heat can be related to the energy required for a phase change in the sample.

Figure 4.11(d) shows the DSC results of the 20% acacia char composite, from the graph we observe that heat was being released from the sample from room temperature to 180°C. However, the trend was reversed; we observe that as the temperature increases the heat being released decreases. An endothermic reaction occurred at 181°C to 888°C, the heat absorbed by the sample above 180°C was rapid. The rapid absorbing of heat can be related to the energy required for a phase change in the sample.

(a) (b)

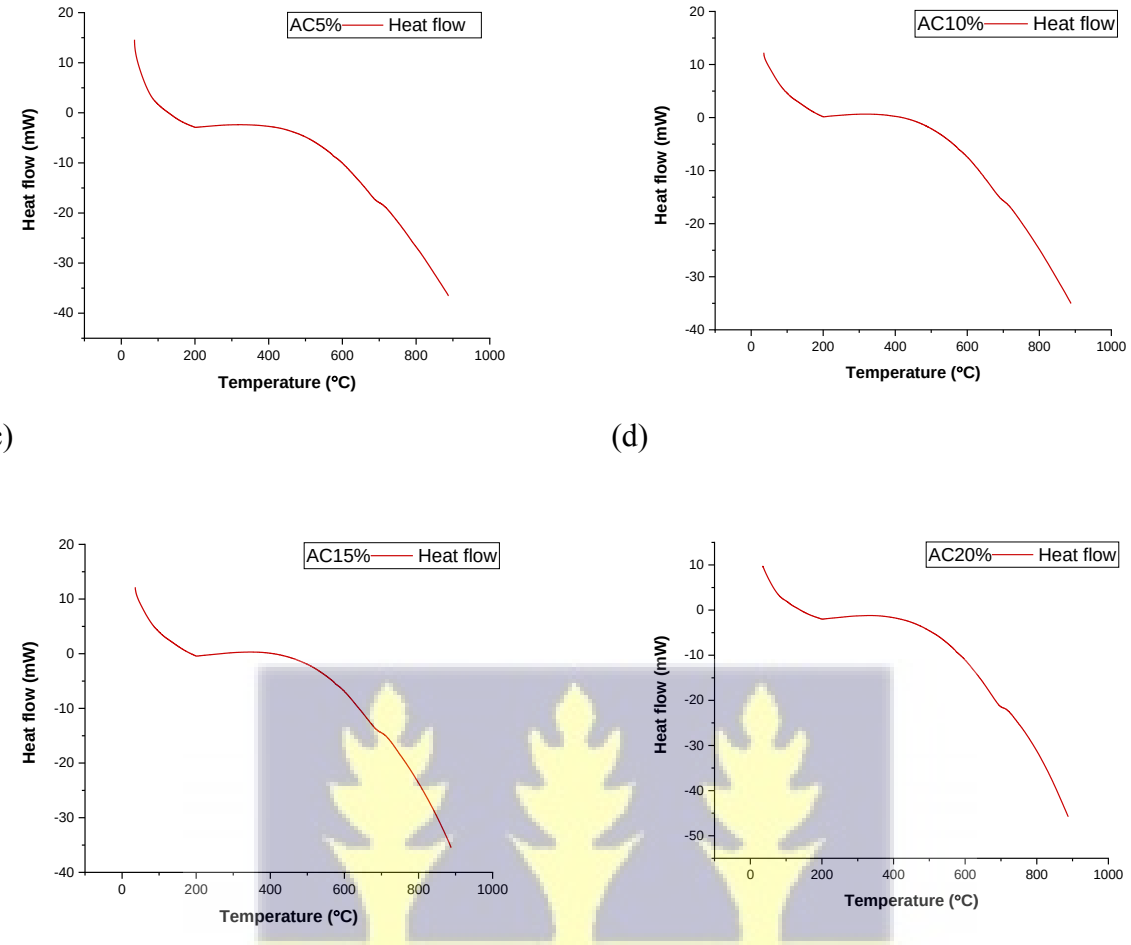

Figure 4.11: DSC Results for Acacia Char composite (a) 5% Addition (b) 10% Addition (c) 15% Addition (d) 20% Addition

4.3.5 Microscopic Images

4.3.5.1 Control samples

Figure 4.12 (a) shows the micrograph with a magnification of 20X of the cross-section of the control sample while (b) shows the micrography of the surface of the composite. The circled portion of image A&B shows a homogenous mix of calcined clay and Portland cement in the internal section and surface respectively and the triangle quartz from the clay. However, there were micro-cracks in the cross-section area captured in the oval shaped area in Figure 4.12 (a-b). This might have occurred due to the compressive strength test conducted on the sample.

The white spots and red portions within the rectangle are quartz and iron oxide from the clay.

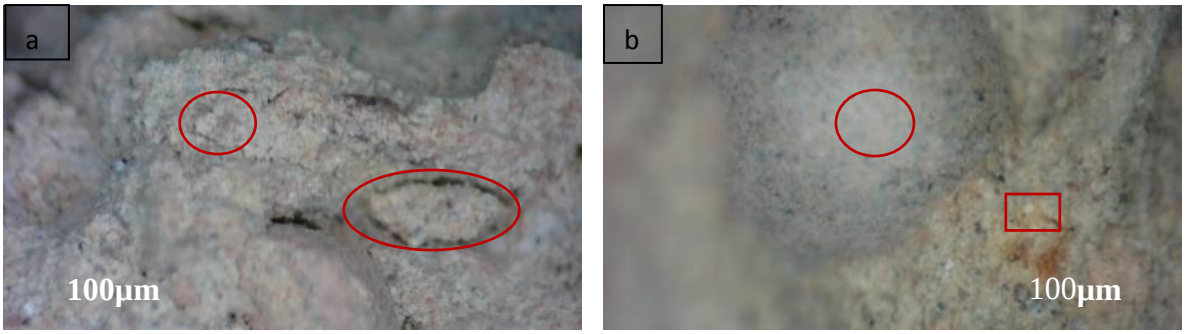

Figure 4.12: Microscopic image of the Control sample (a)cross-sectional area (b)surface of the composite

4.3.5.2 Palm kernel Char-Calcined Clay-Cement Composite

The microscopic images for the palm kernel char 5%, 10%, 15% and 20% composites with a magnification of 20X can be found in Figure 4.13(a-d). From the micrograph we identify the rectangle areas as the palm kernel char, circle area as calcined clay-cement-char mixture, oval areas as iron oxide from the calcined clay material, triangle area as quartz from the clay and pentagon area as pores within the composite. The presence and spread of palm kernel char within the matrix of the composite might have contributed to the good thermal energy harvesting characteristics and compressive strength of the composite. It is important to also note that the energy harvesting characteristics of the composite is also due to the thermal properties of the char.

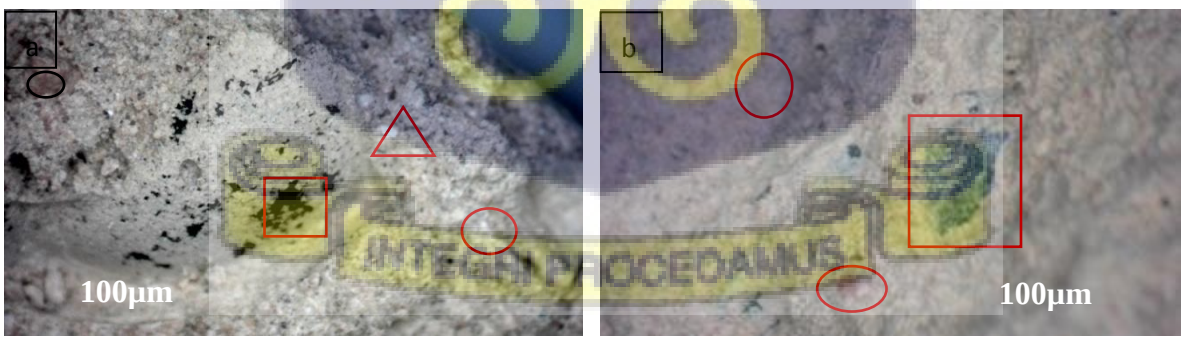

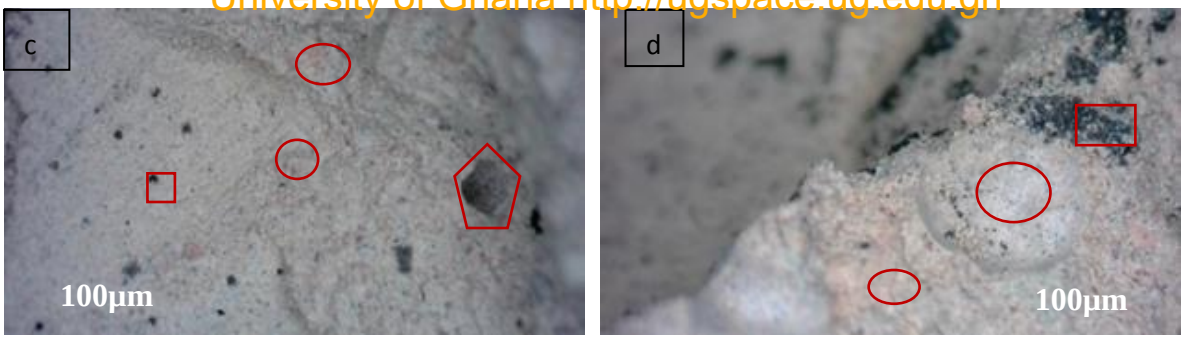

Figure 4.13: Microscopic image of Palm kernel char composites (a) 5%, (b)10%, (c) 15%, (d) 20%

4.3.5.3 Coconut Char-Calcined Clay-Cement Composite

Figure 4.14 shows the cross-section of the coconut shell char composite, the rectangle, triangle, oval, circle, and pentagon marked areas are identified as the coconut char, quartz, iron oxide from the clay, calcined clay-cement-char mixture, and pores within the composite respectively. The presence of the char in the composite corroborates with the good thermal energy harvesting characteristics of the composite. The micrograph also shows an increase in the quantity of char from Figure 4.14(a-d), and this corroborates with the composition and explains the low compressive strength values recorded due to low density of the chars and defects created within the composite. It can also be observed that the composite is homogenously mixed, however a few porous were present in the composite and that might contribute to the low strength value of the composite. The images are a magnification of 20X.

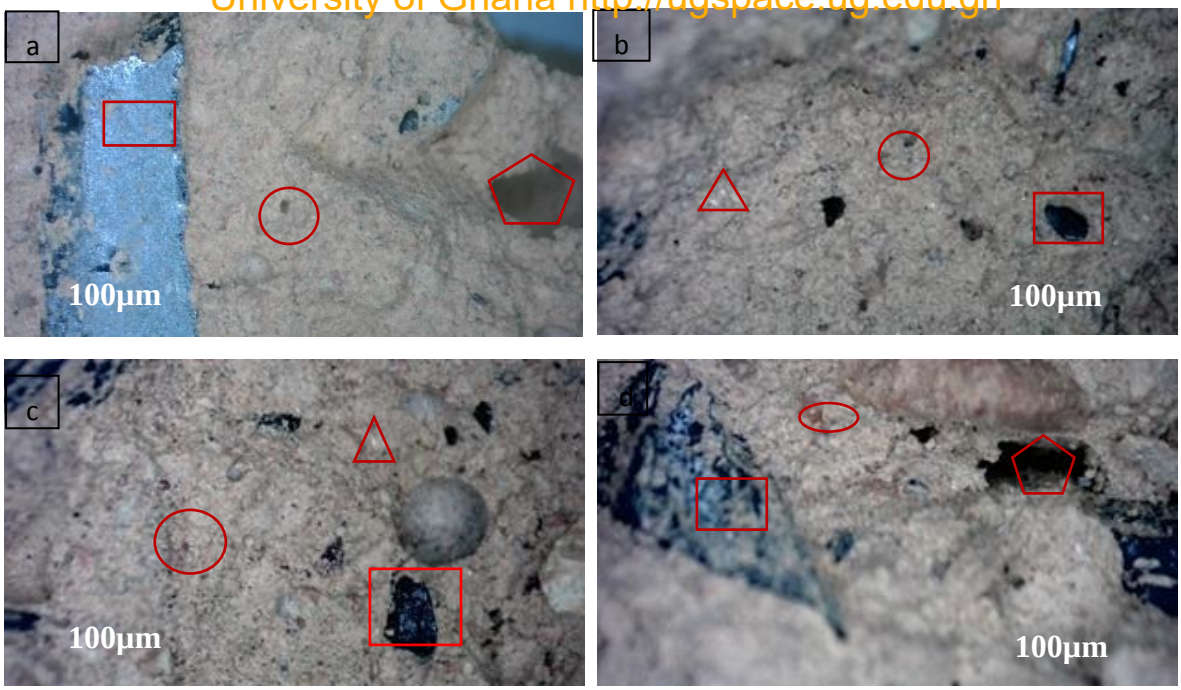

Figure 4.14: Microscopic image of Coconut shell char composites (a) 5%, (b) 10%, (c)15%, (d)20%

4.3.5.4 Acacia Char-Calcined Clay-Cement Composite

The micrography in Figure 4.15 shows the cross-sections of the acacia char composites. The microscopic images identify four items that is quartz form the clay, acacia char, a mixture of calcined clay-cement-char and pores within the composite. These areas are marked with a triangle, rectangles, circles, and a pentagon respectively. The microscopic images show a homogenous mixture and an increase in the char content from (a-d). The char is dispersed within the clay-cement matrix. The presence of char and its high content as the ratio increases confirms the good thermal energy harvesting characteristics and low compressive and flexural strength of the composite respectively.

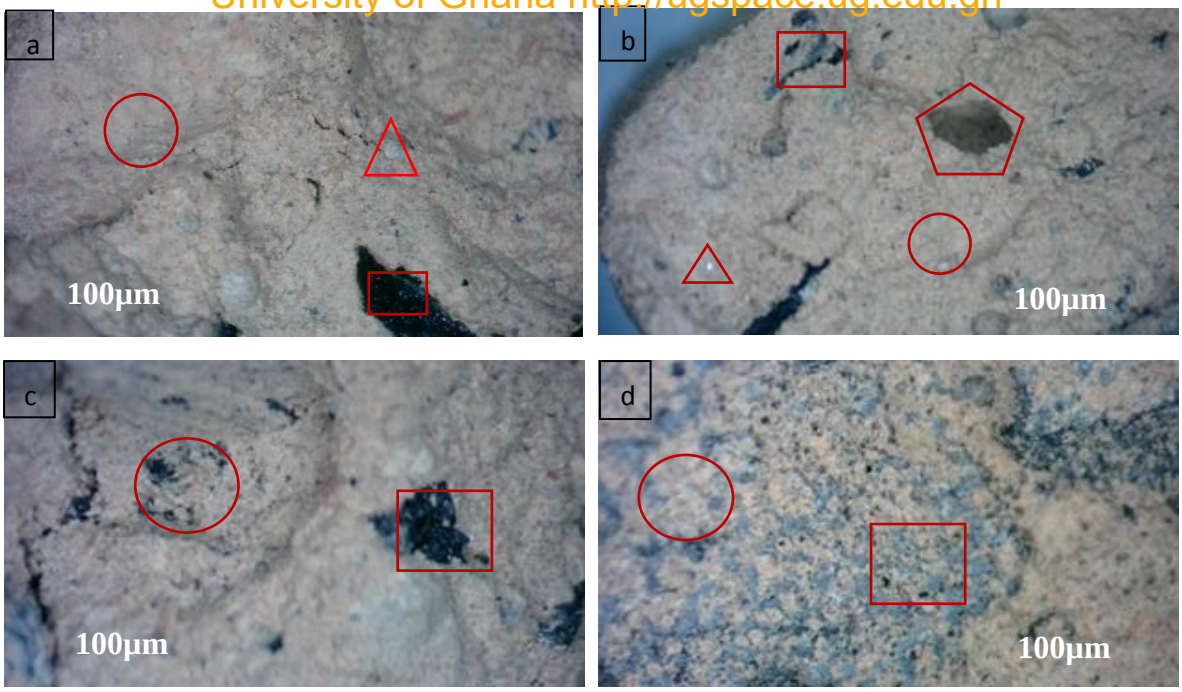

Figure 4.15: Microscopic image of Acacia char composites (a) 5%, (b)10%, (c) 15%, (d) 20%

4.4 Finite Element Analysis (FEA) of Agrowaste Char –Calcined Clay Composites

To understand the mechanical and thermal behavior of the agrowaste char-calcined clay composites, finite element modeling (FEM) was performed, and their mechanical and thermal stress distributions are presented in Figure 4.16(a-h) for the control, palm kernel, coconut shell and acacia char composites showing the surfaces and volume temperatures. Figure 4.15(a) represents the control sample in a time-dependent mode after 12 hours, the surface temperature and volume temperature of the brick while (b) is the isothermal heat flow for the control composite. Properties such as Poisson ratio, thermal conductivity, density, and the specific heat capacity of the materials used were considered in the simulation. For the exterior surface of the brick, a temperature of 37^{o}C (310 K) was recorded and 29^{o}C (302 K) for the interior surface. A temperature difference of ~8^{o}C implies that heat traveled faster on the outer surface than the inner surface indicating that the brick is much thermally stressed since that part is in direct contact with the heat source. As heat is transferred through the

brick via conduction with a constant thermal conductivity, the heat transfer becomes proportional to the temperature gradients in the system. The simulation shows that the control sample has a high heat transfer rate in the inner surface of the brick.

Figure 4.16(c-d) is a 3-D image showing the simulation results of the outer temperature profile and inside temperature distribution of the palm kernel-calcined clay-composite material. This model is to investigate the thermal heat flow in the composite brick and its potential to be used in building as thermal energy storage materials. In this study the model is time-dependent and a simulation period of 12 hours. The temperature on the surface of the brick is 35^{o}C (310 K) and the interior wall temperature of 21^{o}C (294 K), a reduction of 14 K in temperature. The results show that a conducive and comfortable room temperature can be maintained. The reduction in temperature can be attributed to the characteristics of the palm kernel-calcined clay-composite materials. Considering the composite brick model for building applications, the side of the brick with higher thermal temperature will be directed towards the outside of the building, exposing it to the sun. As the sun shines on the surface of the brick, the temperature rises, and the heat is conducted through the brick. For this study the heat transfer module describes conduction where the thermal conductivity is constant. The heat transfer is proportional to the temperature gradients in the system; hence the room temperature will be lower creating thermal comfort. The thermal comfort occurs due to the transfer of heat to the indoor air via convection and to the indoor surfaces via radiation. From the simulation results in Figure 4.16(c) it was observed that parts of the brick are indicated with different colours, these colours illustrate how thermally stressed the region of the composite brick is. Figure 4.16 (d) is the isothermal heat flow of the palm kernel char composite.

Simulation results for the surface and volume temperature for the coconut shells-calcined clay cement composite is shown in Figure 4.16 (e–f). Figure 4.16 (e) shows the surface

temperature and volume temperature of the brick while (f) is the isothermal heat flow. The study of the model is time-dependent, and the simulation was done for 12 hours. For the exterior surface of the brick a temperature of 37^{o}C (310 K) was recorded and 21^{o}C (294 K) for the interior surface. A temperature difference of 16^{o}C was recorded because the composite material was used. The exterior surface is represented in red, while the interior surface is represented in blue; the outer surface of the brick is more thermal stressed since that part is in direct contact with the sun. As heat is transferred through the brick via conduction with a constant thermal conductivity the heat transfer becomes proportional to the temperature gradients in the system. Thermal comfort occurs due to the transfer of heat to the indoor air via convection and to the indoor surfaces via radiation. This thermal comfort occurs due to the energy harvesting characteristics of the composite brick. From the simulation results it can be identified that the brick underwent a lot of thermal stress as a lot of fissures can be seen on the sides of the brick.

The simulation results in Figure 4.16 (g) represent the surface temperature composite and (h) the isothermal heat flow of the acacia char. A temperature of 37^{o}C and 21^{o}C were recorded for the exterior and interior surfaces respectively. The simulation results showed that heat transfer from the exterior to the interior for the acacia char composite was slow compared to the other composites. This can be attributed to the lower thermal conductivity value of the acacia char, hence the ability of the composite to attain thermal comfort. The study of the model is time-dependent, and the simulation was done for 12 hours.

(a)

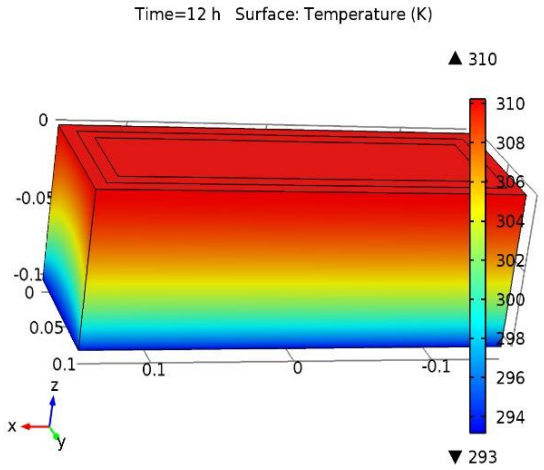

(b)

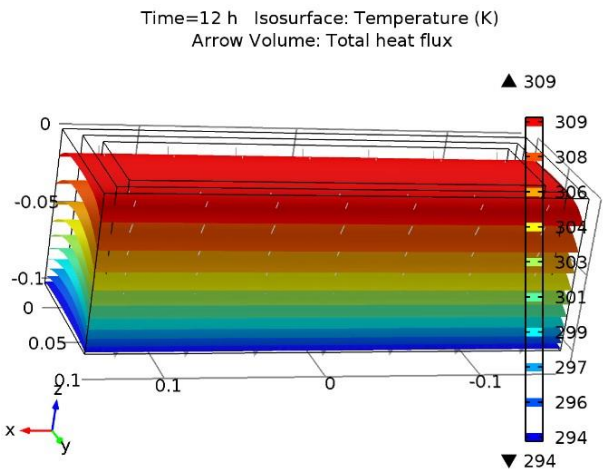

(c)

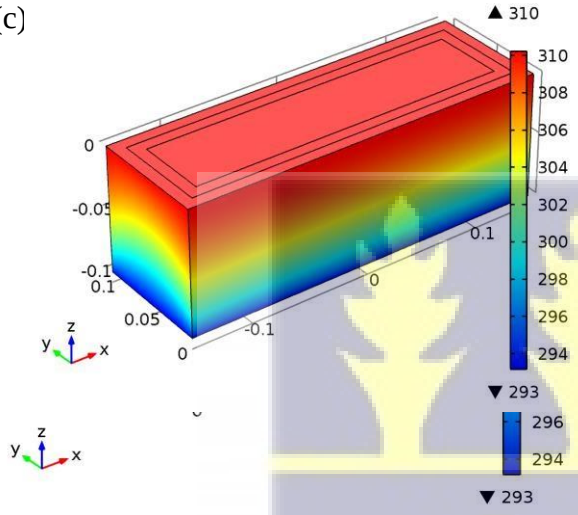

(d)

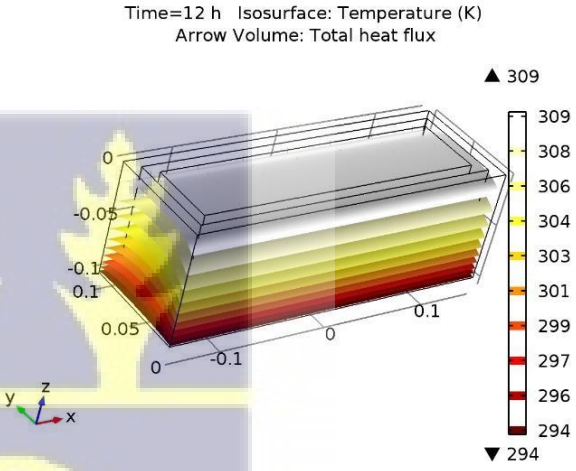

(e)

(f)

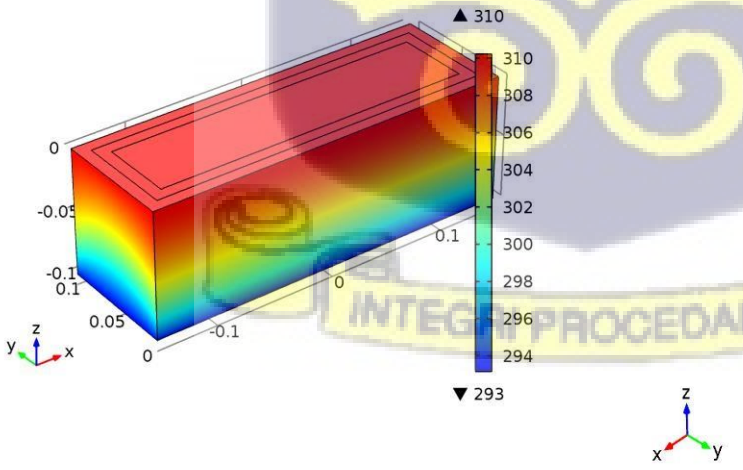

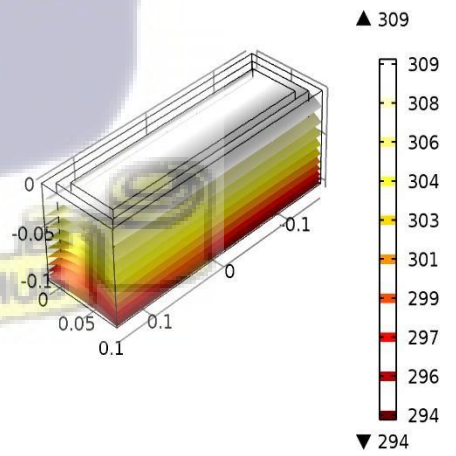

(g)

(h)

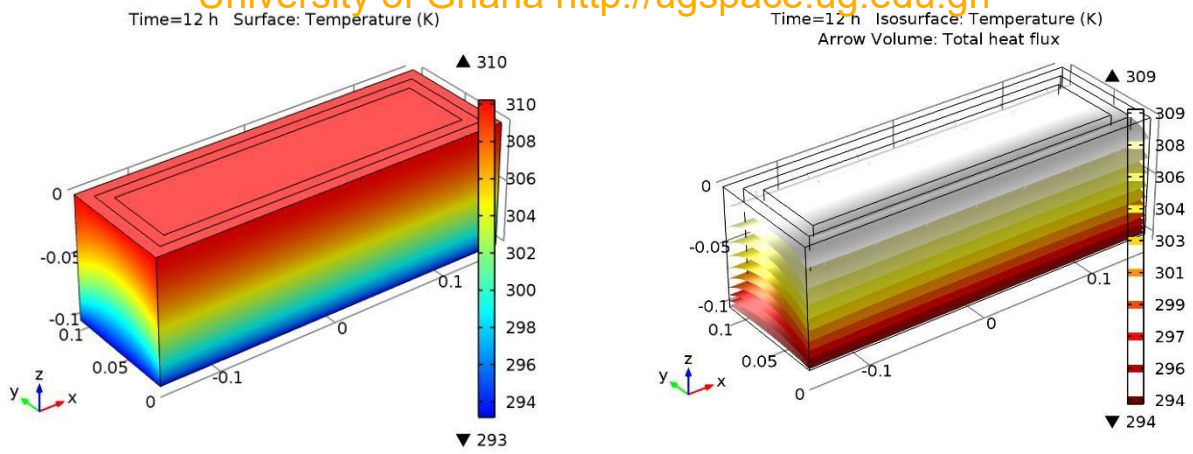

Figure 4.16:(a) Simulation results of surface temperature for Control composite (b) Isothermal Contours of Heat Flow for Control composite (c) Simulation results of surface temperature Palm kernel composite (d)) Isothermal Contours of Heat Flow for Palm kernel composite (e) Simulation results of surface temperature for Coconut composite (f) Isothermal Contours of Heat Flow for Coconut composite (g) Simulation results of surface temperature for Acacia composite (h) Isothermal Contours of Heat Flow for Acacia composite

CHAPTER 5

CONCLUSIONS AND RECOMMENDATIONS

5.1 Conclusions

The aim of the study was to produce a building material with good energy harvesting characteristics and reduce the level of pollution during the raw material acquisition, product development and its use from calcined Abonko clay reinforced with char (palm kernel shells, coconut shells and acacia), investigate its mechanical and thermal properties, and simulate its mechanical and thermal stress distribution. The study results showed that building materials made from calcine clay and char have very good thermal energy harvesting characteristics. The palm kernel shell char composites (5%, 10% and 15%) recorded compressive strength values of ~ 4.60, 4.23, 4.14 N/mm^2 respectively, higher amongst the char composite while the control sample recorded a value of ~ 7.62 N/mm^2 as its compressive strength. These values are higher than the minimum requiring compressive strength for building bricks. Generally, the compressive strength values reduced as the char content increased. TGA results show that the composites have high thermal stability at high temperatures. And the simulation results show that the composites that contain char help attain thermal comfort in rooms.

5.2 Recommendations

The following are recommended:

- Further work should be done to improve the mechanical properties of the coconut shell and acacia char composites.
- SEM analysis should be carried out to further understand the microstructure, surface topography and composition of the composites.
- Investigate the influence of particle size of the char on the energy harvesting characteristics.

REFERENCES

A., S., Kovler, K., Grader, G. S., & Shter, G. E. (2003). The effect of dehydroxylation/ amorphization degree on pozzolanic activity of kaolinite. *Cement and Concrete Research 33*, 405.

Aigbodion, V. S., Hassan, S. B., Olajide, S. O., Agunsoye, O. J., AbdulRahaman, A. S., & Okafor, G. E. (2008). The use of rice husk ash as an aggregate for foundry sand production in Nigeria. *Nigerian Metallurgical Society Annual conference*, (pp. 16-22).

Al-Juboury, A. I. (2009). *Acta Geologica Polonica 59(2)*, 269-282.

Ambroise, J., Murat, M., & Pera, J. (1985). Hydration reaction and hardening of calcined clays and related minerals V: Extension of the research and general conclusions. *Cement and Concrete Research, volume 15(2)*, 261-268.

Appiah, M., Indome, A., & Fudzi, A. A. (2014). *Springer Science., 2014, 55(2)*, 143 – 147.

B.T. Billhall, & Partyka, J. (2011). Technological Study and Characterisation of Clay from the Central Region of Ghana. *Interceram 03-04*, 184-188.

Badogiannis E., Kakali, G., & Tsivilis, S. (2005). Metakaolin as supplementary cementitious material. *Journal of Thermal Analysis and Calorimetry 81*, 457.

Bediako, M., Gawu, K. S., Adjaottor, A. A., Ankrah, J. S., & Atiemo, E. (2016). Analysis of cofired clay and palm kernel shells as a cementitious material in Ghana. Case Stud. *Construc. Mat. 5*, 46–52.

Billhall B.T., & Partyka, J. (2011). Technological Study and Characterisation of Clay from the Central Region of Ghana. *Interceram 03–04*, 184-188.

Billhall, B. T., & Partyka, J. (2011). Technological Study and Characterisation of Clay from the Central Region of Ghana. *Interceram 03–04*, 184-188.

Brown, M. (2007). *Introduction to thermal analysis:Techniques and application , second edition.* New York: Chapman and Hall.

Carrier M, Hardie , A., Uras, U., Görgens , J., & Knoetze , J. (2012). Production of char from vacuum pyrolysis of South-African sugar cane bagasse and its characterization as activated carbon and biochar. *Journal of Analytical and Applied Pyrolysis volume 96*, 24-32.

Cofie O., Rao, K. C., Fernando, S., & Pau, J. (2009). *Composting experience in developing countries:Drivers and constraints for composting development in Ghana, India, Bangladesh and Sri Lanka.* World Bank.

Cai H, Cui D, Li Y, Chen X, Zhang L, Sun J. Apparatus for measuring the seebeck coefficients of highly resistive organic semiconducting materials. Rev Sci Instrum 2013; 84: 044703.

Dollfus P, Nguyen VH, Saint-Martin J. Thermoelectric effects in graphene nanostructures. J Phys-Condens Mat 2015; 27(13): 133204.

Daud, W., Ali, W. S., & Sulaiman, M. Z. (2000). The effects of carbonization temperature on pore development in palm-shell-based activated carbon. *Carbon 38*, 1925–1932.

Dayananda, N., KerthiGowda, B., & Easwara Prasad, G. (2018). A study on compressive strength attributes of jute fiber reinforced cement concrete composite. *IOP Conf.Series: Materials science and engineering 376*.

Enescu, D. (2019). Thermoelectric Energy Harvesting: Basic Principles and Applications. *Green Energy Adv*.

Fackler, K., Stevanic, J., Ters, T., Hinterstoisser, B., Schwanninger, M., & Salmen, L. (2011). FT-IR imaging spectroscopy to localise and characterise simultaneous and selective white-Rot Decay within sprude woodcell. *Holzforschung 65*, 411 - 420.

F. Kuznik, J. V. (2011). In-Situ Study of Thermal Comfort Enhancement in a Renovated Building Equipped with Phase Change Material Wallboard. *Renewable Energy 36 (5*, 1458-1462.

Fernandez, R., Martrena, F., & Scrivener, K. L. (2011). The origin of the pozzolanic activity of calcined clay minerals: A comparison between kaolinite, illite and montmorillonite. *Cement and Concrete Research, Vol 41, No. 1*, 113-122.

Fisher, T., Hajaligol, M., Waymack, B., & Kellog, D. (2002). Pyrolysis behavior and kinetics of biomass derived materials. *J. Anal. Appl. Pyrolysis 62*, 331–349.

Ghosh, S., Harish, S., Rocky, K., Ohtaki, M., & Saha, B. (2019). Graphene enhanced thermoelectric properties of cement based composites for building energy harvesting. *Energy Build* , 202.

Gibson, R. (2010). A review of recent research on mechanics of multifunctional composite materials and structures. *Compos. Struct. 92 (12)* , 2793- 2810.

González AS, Plaza ,, M., Rubiera , F., & Pevida , C. (2013). Sustainable biomass-based carbon adsorbents for post-combustion CO2 capture. ;. *Chemical Engineering Journal 230*, 456-65.

Hasnain, S. M. (1993). *Energex '93, Proc. 5th Intl. Energy Conference.* Seoul, Korea.

Hasnain, S. M. (1998). Review On Sustainable Thermal Energy Storage Technologies, PART I. *Heat Storage Materials and Techniques Energy Convers. Mgmt Vol. 39, No. 11*, 1127-1138.

Hasnain, S. M. (1998). Review On Sustainable Thermal Energy Storage Technologies, PART I. *Heat Storage Materials and Techniques Energy Convers. Mgmt Vol. 39,*, 11271138,.

He, C., Osabaeck, B., & Makovicky, E. (1995). Pozzolanic reactions of six principal clay minerals: Activation reactivity assessments and technological effects. *Cement and Concrete Research 25*, 1691.

Hohne, G. W., Hemminger, W. F., & Flammersheim, H. J. (2003). *Differential Scanning Calorimetry*. Berlin, Heidelberg: Springer.

Hoornweg, D., & Bhada-Tata, P. (2012). What a waste:A global review of solid waste management. *Urban development series; knowledge papers no. 15*. Washington DC: World bank.

Huang S, Li X, Liu F, Chang J, Xu D, Cheng X. Effect of carbon black on properties of 0-3 piezoelectric ceramic/cement composites. Curr Appl Phys 2009; 9(6): 1191-1194.

Kakali, G., Perraki, T., Tsivilis, S., & Badogiannis, E. (2001). Thermal threatment of kaolin: the effect of mineralogy on the pozzolanic activity. *Applied clay science*, 73-80.

Kenisarin, M., & Mahkamov, K. (2016). Passive thermal control in residential buildings using phase change materials. *Renewable and Sustainable Energy Reviews, Volume 55* , 371-398.

Khiari, B., Jeguirim, M., Limousy, L., & Beennici, S. (2019). Biomass derived chars for energy applications. *Renewable and sustainable energy reviews. Elsevier vol. 108(C)*, 253-273.

Kuznik, F., Virgone, J., & Johannes, K. (2011). In-Situ Study of Thermal Comfort Enhancement in a Renovated Building Equipped with Phase Change Material Wallboard. *Renewable Energy 36 (5)*, 1458-1462.

Lee, S., Kim, Y., & Moon, H. (2003). Energy filtering electron microscopy(EF-TEM) study of a modulated structure in metakaolinite represented by a 12Armstrong modulation. *journal of American ceramic society, 86*, 174 -176.

Lombardi, K. C. (2002). Structural and morphological characterization of the PP-0559 kaolinite from the Brazilian Amazon region. *Journal of the Brazilian Chemical Society 13*, 2.

Luciana Sucupira, J. C.-G. (2021). Review of Energy Harvesting for Buildings Based on Solar Energy and Thermal materials. *CivilEng*, 854-873.

Liu L, Knapp M, Ehrenberg H, Fang L, Fan H, Schmitt LA, Fuess H, Hoelzel M, Dammk H, Thi MP, Hinterstein M. Average vs. local structure and composition property phase diagram of $K_{0.5}Na_{0.5}NbO_3$-$Bi_{½}Na_{½}TiO_3$ system. J Eur Ceram Soc 2017; 37(4): 1387-1399.

Mackay, D., & Roberts, P. V. (1982). The influence of pyrolysis conditions on the subsequent gasification of lignocellulosic chars. *Carbon 20 (2)*, 105–111.

Mahanim, S., Asma, I. W., Rafidah, J., Puad, E., & Shaharuddin, H. (2011). Production of activated carbon from industrial wastes. *J. Trop. For. Sci.,23*, 417-424.

Miezah, K., Obiri-Danso, K., Fei-Baffoe, B., Kadar, Z., & Mensah, M. Y. (2015). Municipal solid waste characterization and quantification as a measure towards effective waste management in Ghana. *Waste Management, 46*, 15–27.

Miezah, K., Obiri-Danso, K., Kadar, Z., Fei-Baffoe, B., & Mensah, M. Y. (2015). Municipal solid waste characterization and quantification as a measure towards effective waste management in Ghana. *Waste Management, 46*, 15–27.

Mitchell, J. (2005). *Fundamentals of Soil Behaviour, 3rd edition.* New York: John Wiley & Sons, Inc.

Mohamed Shameer P., M., & Mohamed, N. P. (2019). Exploration and enhancement on fuel stability of biodiesel. *Applications, Technologies and Environmental Sustainability*, 181-213.

Naresh Marturi, S. D. (2014). Scanning electron microscope image signal-to-noise. *The Journal of Scanning Microscopies*, 1-11.

Norgate TEL, D. (2009). Environmental and economic aspects of charcoal use in steelmaking. *ISIJ International, 49*, 587-95.

Ofosu-Badu, K., & Sarpong, D. (2013). *Oil palm industry growth in Africa: a value chain and smallholders' study for Ghana, in Rebuilding West Africa's Food Potential. In: Elbert, A. (Ed.).* FAO/IFAD.

P.E. Grattan-Bellew. (1996). Microstructural investigation of deteriorated Portland cement concretes, . *Constr. Build. Mater. 10 (1)*, 3 – 16.

Perez-Lombard, L., Ortiz, J., & Pout , C. (2007). A review on buildings energy consumption information. *Energy and Buildings 40 (2008)*, 394–398.

Prusty J. K., Patro, S. K., & Basarka, S. S. (2016). "Concrete using agro-waste as fine aggregate , for sustainable built environment – A review. *Int. J. Sustain Built Environ., vol. 5, no. 2,*, 312–333.

Ramakrishnan, S., Wang, X., Sanjayan, J., & Wilson, J. (2017). Thermal performance of buildings integrated with phase change materials to reduce heat stress risks during extreme heatwave events. *Applied Energy, Volume 194*, 410-42.

Reindel, D. T. (1996). Sustainable Thermal Energy Storage. *EPRI Intl. Conf. in Proc.* Minnesota, USA,.

Riyadh. (1997). *Conservation and Load Management.* Saudi Arabia: King Abdulaziz City for Science and Technology (KACST).

Rodrigo, F., Martirena, F., & Scrivener, K. L. (2011). The origin of the pozzolanic activity of calcined clay minerals: A comparison between kaolinite, illite and montmorillonite. *Cement and Concrete Research 41*, 113–122.

Selvam, S. A. (2019). *Energy Harvesting Routing Algorithm for RFID Sensor Transponder.*

Singh M., & Grag, M. (2006). Reactive pozzolana from Indian clays–Their use in cement mortars. *Cement and Concrete Research 36*, 1903.

Starovoytova, D. (2018). Solid Waste Management (SWM) at a University Campus (Part 1/10): Comprehensive review on legal framework and background to waste management, at a global context. *Journal of Environment and Earth Science, 8(4)*, 68–116.

Sybertz, F. B. (1993). Assessment of the effectiveness of Coal Fly Ash as a Concrete Addition. *Beuth Verlag*, 111. Thermoelectric energy harvesting using cement-based composites: a review. (n.d).

Tsai, W. T., Lee, M. K., & Chang, Y. M. (2006). Fast pyrolysis of rice straw, sugarcane Bagasse and coconut shell in an induction-heating reactor. *J. Anal. Appl. ,Pyrolysis 76(12)*, 230 – 237.

Uchimiya M, L. I. (2010). Immobilization of heavy metal ions (CuII, CdII, NiII, and PbII) by broiler litter-derived. *Journal of agricultural and food chemistry*, 38-44.

Uchimiya M, Lima, I., Thomas, K. K., Chang , S., Wartelle , L., & Rodgers, J. (2010). Immobilization of heavy metal ions (CuII, CdII, NiII, and PbII) by broiler litterderived. *Journal of agricultural and food chemistry*, 38-44.

V., M. M., Ralegaonkar, R. V., & Mandavgane, S. A. (2013). Application of agro-waste for sustainable construction materials: A review. *Constr. Build. Mater., vol. 38*, 872–878.

V.P. Singh, M. K. (2021). Thermoelectric energy harvesting using cement-based composites: a review. *Materials Today Energy 21* .

Vergara, S. E., & Tchobanoglous, G. (2012). Municipal Solid Waste, and the Environment: A Global Perspective. *Annual Review of Environment and Resources, Vol. 37*, 277-309.

Wang, H., Jasim, A., & Chen, X. (2018). Energy harvesting technologies in roadway and bridge for different applications—A comprehensive review. *Appl. Energy 212*, 1083–1094.

Wargorcki, P., Seppanen, O., Andersson, J., Boerstra, A., Clements-Croome, D., Fitzner, K., & Hanssen, S. (2006). *REHVA Guidebook No. 6: indoor climate and productivity in offices- how to intergrate productivity in life-cycle analysis of building services.* Rue Washington: REHVA.

Xiu S, Shahbazi , A., & Li , R. (2017). Characterization, Modification and Application of Biochar for Energy Storage and Catalysis: A Review. *Trends in Renewable Energy;3*, 86-101.

Xu, F., Yu, J., Tesso, T., Dowell, F., & Wang, D. (2013). Qualitative and quantitative analysis of lignocellusic biomas using infrared techniques: a mini review. *Applied energy 104*, 801 - 809

Yao, Y., Gao, B., Inyang, M., Zimmerman, A., Cao, X., & Pullammanappallil, P. (2011). Biochar derived from anaerobically digested sugar beet tailings: Characterization and phosphate removal potential. *Bioresource Technology;102*, 6273-8.

Yaya, A., Asamoah, R., Nyankson, E., Annan, E., Agyei-Tuffour, B., Efavi, J., Onwona-Agyeman, B. (2018). Industrial applications of clay minerals from Ghana (A review). *Orient. J. Chem., vol 34(4)*, 1719-1734.

Zhang C, Geng , Z., Cai , M., Zhang , J., Liu, X., & Xin , H. (2013). Microstructure regulation of super activated carbon from biomass source corncob with enhanced hydrogen uptake. *International Journal of Hydrogen Energy; 38 (22)*, 9243-50.

Zhou, D., Zhao, C., & Tian, Y. (2012). Review on thermal energy storage with phase change materials in building applications. *Applied Energy*, 593-605.